Imprint Lithography using Nanocrystalline CVD Diamond Molds

B.H.L. Overes

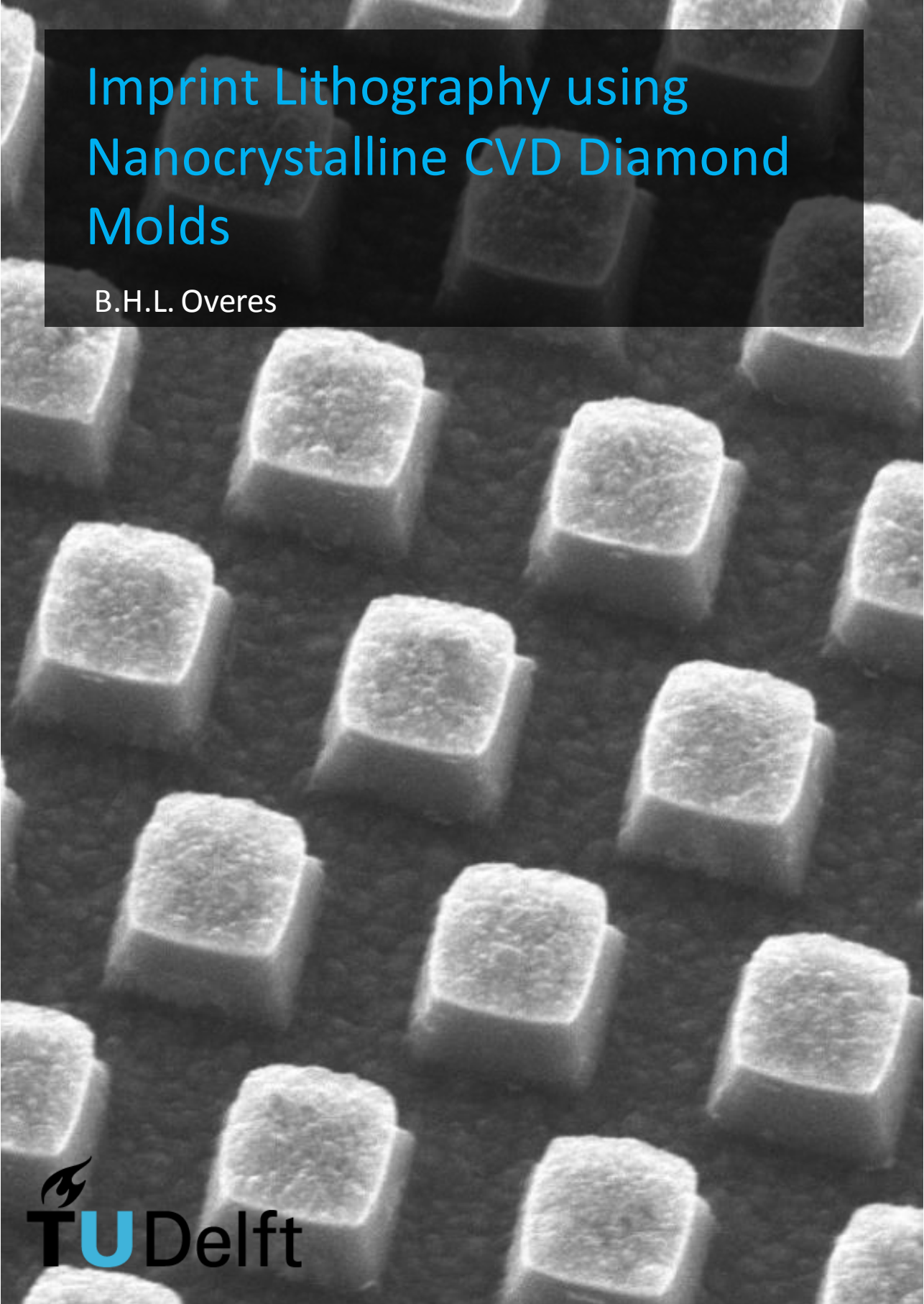

TU Delft

Department of Precision and Microsystems Engineering

Imprint Lithography using Nanocrystalline CVD Diamond Molds

B.H.L. Overes

Report no : 2018.005
Coaches : Dr. J.G. Buijnsters & Dr. A.F. Sartori
Professor : Prof.dr. G.C.A.M. Janssen
Specialisation : Micro & Nano Engineering
Type of report : Master Thesis
Date : 28-02-2018

Imprint Lithography using Nanocrystalline CVD Diamond Molds

by

B.H.L. Overes

to obtain the degree of Master of Science
at the Delft University of Technology,
to be defended publicly on Wednesday February 28, 2018 at 9:45 AM.

Student number:	4243226
Supervisors:	Dr. J.G. Buijnsters & Dr. A.F. Sartori
Thesis committee:	Prof. dr. G.C.A.M. Janssen
	Dr. D. Dodou

This thesis is confidential and cannot be made public until August 1, 2018.

TU Delft

PREFACE

I would like to thank my supervisors Dr. Ivan Buijnsters and Dr. Andre Sartori for guiding me in the right direction, asking the questions I needed to think through, and helping me with the experimental work. You guys have always been there for me during my thesis, and I greatly appreciate your ability to always provide help on very short notice.

I would like to thank everyone from the MNE department for providing me with valuable insights during the MNE meetings. Furthermore, I would like to thank everyone contributing to the excellent work environment in the office, Heleen Payens, Lili Maxime Hauzer, Ryan van Dommelen, Pieter Kapel, Bart Holtzer, Jelmer de Zeeuw, Elena De Lazzari, Henri van der Deijl, Koen Markestein, Mirando Loonman, Yannick Jansen, and Koen Scheurs.

I want to thank Dr. Paola Fanzio and Dr. Luigo Sasso for sharing with me their wisdom about polymers. I would like to thank Agnieska Kooijman Banaszak for allowing me to use their department's equipment. And of course our PME technicians, Rob Luttjeboer, Spiridon van Veldhoven, Patrick van Holst, and Harry Jansen for always lending me their technical expertise.

I would also like to thank my collaborators from outside TU Delft, Prof.dr. Luis Vázquez from Instituto de Ciencia de Materiales de Madrid for providing me with the micro-structured silicon substrates. Furthermore, Dr. Doris Steinmüller-Nethl from CarbonCompetence has greatly helped me by growing UNCD on our substrates.

Last but not least I want to thank everyone who disagreed with me and thereby provided me with the opportunity to stress test my work and ideas.

Bart Overes
Delft, Februari 2018

ABSTRACT

Micro-/nanoimprint lithography is a high-throughput, high-resolution, and low-cost mass production fabrication process often used for creating microfluidic devices and optical components. In the imprint lithography process, a surface pattern of a stamp is replicated into a material by mechanical contact and three dimensional material displacements. These stamps are exposed to high pressures and temperatures and need to be able to withstand these circumstances in order to be durable. Diamond is potentially the ideal surface material for an imprint lithography stamp, since it has a high hardness, a high thermal conductivity coefficient, a low thermal expansion coefficient, it is chemically inert and highly wear resistant.

Up until now, only molds made completely out of diamond have been used for imprint lithography. These molds were fabricated using single crystal or polished Chemical Vapor Deposited (CVD) diamond, which were then micro-structured by focused ion beam, reactive ion etching or e-beam lithography. Unfortunately, the availability of large area, single crystal diamond is very limited, and therefore extremely costly. On the other hand, diamond synthesis by chemical vapor deposition provides the possibility to deposit polycrystalline diamond films on areas up to tens of cm^2. However, it is a rather slow process where typical growth rates are about 1 μm/hour, and thus production of full diamond stamps is time consuming and expensive.

In this thesis, two new methods for the fabrication of CVD diamond imprint lithography molds have been developed. In the first method, a layer of 0.5 μm CVD diamond is deposited on micro-structured silicon. The second method makes use of porous silicon templates through which diamond can be grown, resulting in micro-structured diamond molds. Since polishing micro-structured diamond layers is not possible, the molds were coated with an anti-adhesion layer in order to facilitate release of the mold after imprinting. Both methods proved to be suited for imprinting into a cyclic olefin copolymer developed by TOPAS (grade 6013). With the first method, imprint dimensions of 1 μm with a depth of 350 nm were realized, and imprint dimensions of 2.5 μm with a depth of 2 μm were realized with the second fabrication method. These new approaches greatly reduce complexity of the fabrication process for durable stamps, and thereby the costs involved in creating imprint lithography stamps.

CONTENTS

List of Figures

LIST OF TABLES

1

INTRODUCTION & RESEARCH FOCUS

Over the last decades, there has been a continuous drive to fabricate components that are smaller and smaller. This enables the fabrication of compacter devices that are more efficient, faster, require less power, and are capable of performing more functions. In order to meet the demands of the consumers, techniques for the production of these tiny components have to be developed and improved continuously. One of the techniques for the fabrication of tiny components is imprint lithography.

In the imprint lithography process, the surface pattern of the imprint lithography mold is transferred to the imprint material by mechanical contact and three dimensional material displacements. This enables to pattern a wide variety of materials, since one is no longer dependent on the availability of a good etch as is the case with commonly used production methods. One of the drawbacks of imprint lithography is the relatively short life-span of the molds, often fabricated out of silicon.

A seemingly ideal material for imprint lithography molds is diamond, due to its high hardness, high thermal conductivity, low thermal expansion coefficient and its great wear resistance. However, production of micro-structured diamond imprint lithography molds is far from simple. Up until now, diamond molds have been produced by synthesizing thick diamond layers, which are then polished and patterned. Common methods for patterning diamond are Focused Ion Beam (FIB), Reactive Ion Etching (RIE) and e-beam lithography, but these processes are slow and costly.

This thesis will focus on the development of Chemical Vapor Deposited (CVD) diamond imprint lithography mold fabrication methods, in which no polishing and patterning steps are required after CVD diamond synthesis. This would greatly reduce time and costs involved in the production of CVD diamond imprint lithography stamps. Two promising techniques have been explored in this MSc thesis. In the first technique, a thin CVD diamond film is deposited on a micro-structured silicon sample, which designedly provides protection for the silicon underneath and thereby increases the durability of the mold. The second technique focuses on the fabrication of full diamond structures by

synthesizing diamond by CVD through porous templates. The diamond growth is then limited to the pores of the template resulting in the growth of structured diamond molds. Both mold fabrication concepts have been investigated and the resulting diamond imprint lithography stamps have been tested by imprinting into a cyclic olefin copolymer (COC).

RESEARCH GOAL

The goal of this research is the development of simple and fast production methods of thin-film diamond imprint molds through the CVD diamond coating of micro-structured silicon and the use of template-based synthesis.

RESEARCH QUESTIONS

- Can CVD diamond imprint molds be produced by coating micro-structured silicon with a thin film of CVD diamond?
- Can CVD diamond imprint molds be produced by confined growth of diamond through porous silicon templates?
- Are these imprint molds suited for imprinting into COC?

2

SYNTHETIC DIAMOND & NANOIMPRINT LITHOGRAPHY

In this Section, some basics about diamond synthesis and nanoimprint lithography will be discussed together with relevant papers in these fields of study.

2.1. DIAMOND

Due to its valency carbon is capable of forming many different allotropes, such as graphite, graphene, and diamond. Among the various forms of carbon, diamond is a very interesting one because of its many extreme material properties. The five properties most important for this thesis study are: the thermal expansion coefficient ($2 \cdot 10^{-6}$/°C at 25-200°C), thermal conductivity (2100 W/m·K at 25°C), hardness (Vickers hardness ~100 GPa), furthermore diamond is chemically inert and is highly wear resistant [1, 2]. The extreme properties of diamond are mostly a result of its dense lattice, which is a combination of two face centered cubic (fcc) lattices as is shown in Figure 2.1. In this Figure, the black balls represent the carbon atoms, the white sticks depict the C-C covalent bonds between atoms, and the yellow cube frame defines the unit cell.

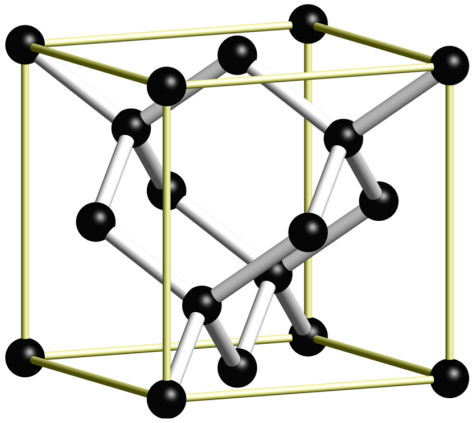

Figure 2.1: Diamond lattice. Adapted from [3].

Natural diamond is formed in a high temperature, high pressure environment at about 140-190 kilometers beneath the Earth's surface. These diamonds are brought to the surface by deep volcanic eruptions. During these deep volcanic eruptions, the diamond is transported by magma which cools down into kimberlites and lamproites near the Earth's surface [4].

Since natural diamond is very uncommon and hard to process, several methods have been developed for diamond synthesis. There are three commonly used methods to synthesize diamond in the lab: High Pressure High Temperature synthesis (HPHT), Chemical Vapor Deposition (CVD) and Detonation synthesis. All three methods will be explained in Section 2.1.2.

Two main classes of synthetic diamond are distinguished, namely monocrystalline diamond and polycrystalline diamond. Monocrystalline diamond, as the name already suggests, consists of one single diamond crystal and is usually produced via the HPHT method. However, large (up to cms) monocrystalline diamonds can also be formed using the CVD process. When products consisting of more than one diamond crystal are being synthesized, the diamond material is referred to as being polycrystalline. Due to the presence of grain boundaries in polycrystalline diamond, the hardness of this type of diamond is lower than the hardness of monocrystalline diamond. However, polycrystalline diamond can be deposited in thin-film form as in done in the CVD process. Polycrystalline diamond will be further elaborated in the next Section.

2.1.1. POLYCRYSTALLINE DIAMOND

As mentioned earlier, diamond consisting of multiple diamond crystals is classified as polycrystalline diamond. These diamond crystals are separated by grain boundaries which consist of sp^2 carbon bonds or disoriented sp^3 carbon bonds. Three main classes of polycrystalline diamond are distinguished: Microcrystalline Diamond (MCD), Nanocrystalline Diamond (NCD) and Ultra Nanocrystalline diamond (UNCD). An overview of the different properties is presented in Figure 2.2. The main difference between the three classes is the size of the diamond crystals, where MCD has the biggest crystals and UNCD

the smallest. Different CVD growth parameters are required to grow the different kinds of polycrystalline diamond.

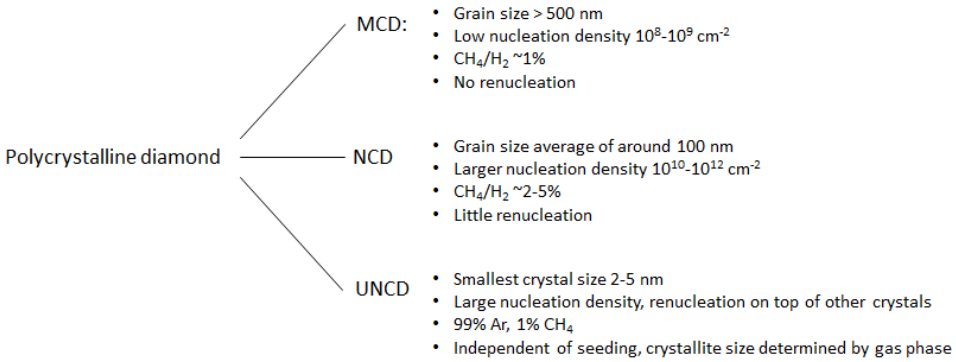

Figure 2.2: Overview of average grain size and main CVD growth conditions for the three different classes of polycrystalline diamond: MCD, NCD, and UNCD.

MCD is defined as diamond consisting of individual grains larger than 500 nm, which are usually referred to as micron size grains. During MCD growth no re-nucleation takes place, the seeds start growing in 3 dimensions until they make contact with other diamond grains. After making mechanical contact, the grains start growing upwards, and in this phase the diamond grains compete for growth so thicker layers will lead to fewer and larger grains at the surface of the diamond layer. MCD has a relatively low nucleation density of about 10^8-10^9 cm^{-2}. When the grain size is on average about 100 nm or smaller and little to no re-nucleation occurs, polycrystalline diamond is classified as NCD. NCD usually is a thin layer (thickness of max. about 2 μm) with no re-nucleation or a thicker layer with small re-nucleation, and the nucleation density is significantly higher than in the case of MCD with values of about 10^{10}-10^{12} cm^{-2}. If there is continuous re-nucleation a UNCD layer forms. Due to this continuous re-nucleation, the grain sizes of a UNCD layer are very small (about 2-5 nm). Furthermore, the content of sp^2 carbon is very low [5, 6].

The average surface grain size has a direct influence on the surface roughness of the diamond layer, as larger crystal size results in a larger surface roughness. Therefore, the roughness of the deposited diamond layer can be tuned to a certain extent by the type of polycrystalline diamond grown [7].

2.1.2. DIAMOND SYNTHESIS

In this section three methods of diamond synthesis will be discussed: HPHT, CVD, and detonation synthesis. Figure 2.3 shows the phase diagram of carbon with growth conditions of the different growth processes.

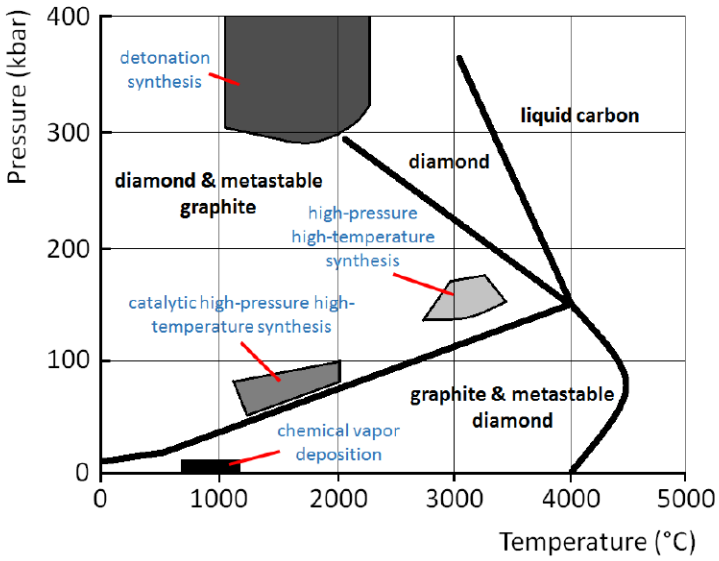

Figure 2.3: Phase diagram of carbon; different diamond growth techniques are presented. Reproduced from [8].

HIGH PRESSURE, HIGH TEMPERATURE SYNTHESIS

HPHT is an abbreviation for high pressure, high temperature and is essentially recreating the environment in which natural diamond grows. This method is only used for the production of monocrystalline diamond mostly using graphite as the high purity carbon source, and it allows to make large (up to several millimeters) diamonds. As can be seen in Figure 2.3 there are two regions where HPHT diamonds are usually grown, i.e. with and without the aid of catalysts. Using a catalyst allows to decrease the pressure and temperature needed for diamond growth. Catalysts are the transition metals such as iron, cobalt, chromium, nickel, platinum and palladium. These metal-solvents dissolve carbon extensively, break the bonds between groups of carbon atoms and between individual atoms, and transport the carbon to the growing diamond surface, typically a small diamond seed. In this way, a relatively large synthetic diamond is formed [2]. Since HPHT synthesis is unsuited for growing diamond on top of substrates, it can not be used to grow thin films of diamond.

CHEMICAL VAPOR DEPOSITION

The second method that can be used to synthesize diamond is Chemical Vapor Deposition (CVD). This is a chemical process often used to deposit thin films of solid material. In the specific case of diamond CVD, an already existing diamond seed is grown further, since nucleation of diamond is very sluggish due to the very high surface free energy of diamond. Because all the seeds exposed to the right conditions will grow further this method is very suited for synthesizing polycrystalline diamond films. Growing monocrystalline diamond is also possible with a CVD tool, however, it is very difficult and will not be further discussed in this thesis. Since Hot Filament Chemical Vapor De-

position (HFCVD) is used in this thesis to synthesize diamond the further explanations will focus on HFCVD.

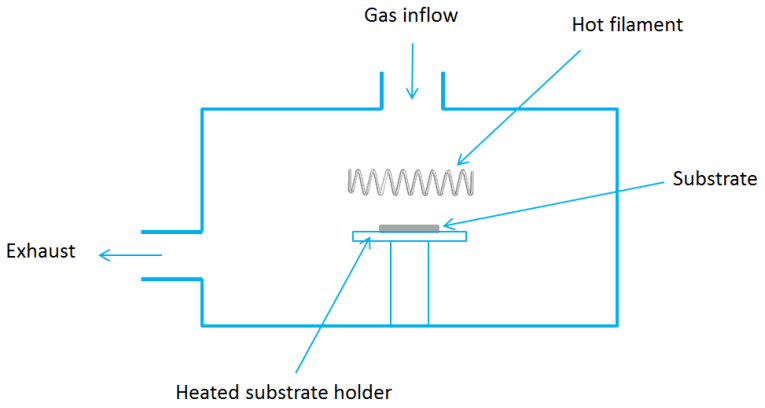

Figure 2.4: Schematic representation of a HFCVD reactor.

HFCVD is a so called thermal induced CVD process, this means that the chemical vapor is activated by hot filaments or hot surfaces, a schematic representation is shown in Figure 2.4. The gases around these heated elements reach a temperature of about 2300 to 2900 K [9]. The temperature of the substrate is preferably in the range from 1000 to 1400 K, because at lower temperatures the deposition rate reduces, and at higher temperatures the growth of graphite dominates. HFCVD of polycrystalline diamond films is typically done at reduced pressure in the range of few to tens of millibars. Thermal induced CVD diamond growth processes generally make use of methane (CH_4) and hydrogen (H_2) in gas form. The primary function of CH_4 is providing C atoms to synthesize diamond, whereas the primary function of H_2 is to terminate the dangling carbon bonds on the surface of the growing diamond layer or diamond nucleus. Furthermore, hydrogen prevents the growth of graphite, atomic hydrogen etches sp^2 carbon bonds (graphite) a lot faster than diamond like sp^3 carbon bonds [10]. A typical CVD diamond growth rate is 1 μm/h.

For diamond to grow CH_4 has to dissociate in other reactive species such as C_2H_2, and CH_3, these two molecules are believed to be the dominant molecules in diamond formation [6]. A schematic representation of diamond growth with CH_3 is shown in Figure 2.5. By using different growth parameters different kinds of polycrystalline diamond can be synthesized. The type of diamond synthesized is mainly dependent on the composition of the gases fed to the reactor. By increasing the CH_4/H_2 ratio the grain size of the film decreases. This leads to a lower surface roughness but also decreases the hardness of the diamond film. An increase of the CH_4/H_2 ratio from about 1% to 2-5% will likely lead to NCD growth instead of MCD growth, further increase of the CH_4 concentration would lead to higher production of sp^2 carbon [6]. While adjusting the CH_4/H_2 ratio leads to smaller grain size, it does not result in the growth of UNCD. UNCD is grown in a hydrogen poor gas mixture usually consisting of 99% Ar and 1% CH_4 [11].

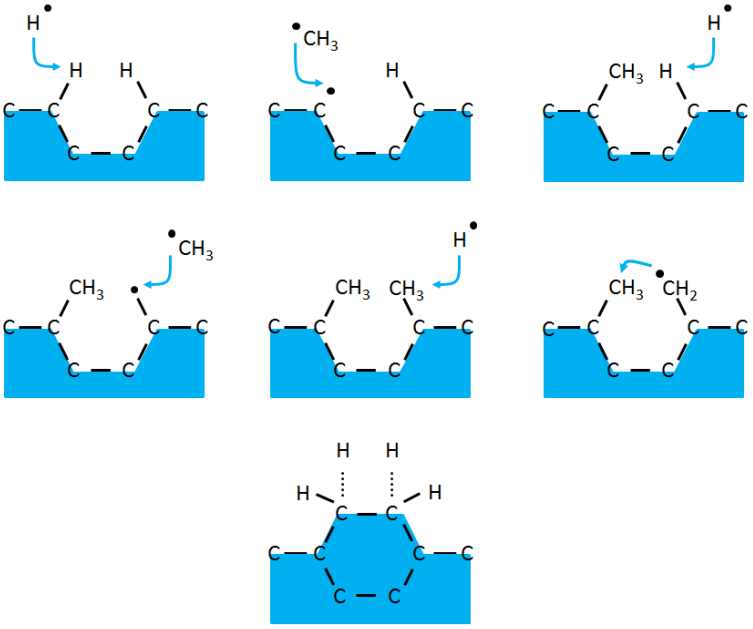

Figure 2.5: Representation of diamond growth with CH_3.

DETONATION SYNTHESIS

Another diamond production method is detonation synthesis, which as the name already uggests, uses detonation of oxygen-deficient explosives, typically mixtures of TNT/RDX, in a closed chamber to form diamond nanoparticles. Detonation synthesis transforms graphitic material into diamond crystallites by using circular shock waves. The diamond particles formed with detonation synthesis have a very narrow size distribution around 5 nm. This narrow distribution is a result of the short period where the thermodynamic factors enable diamond formation. The time of synthesis in the explosion zone does not exceed 0.2-0.5 μs [12]. However, when the pressure drops and temperatures are still elevated graphitic soot is formed. Therefore, the reactor needs to be cooled as fast as possible [13]. Detonation NanoDiamonds (DNDs) are often used as diamond seeds in other diamond synthesis processes such as CVD.

2.2. IMPRINT LITHOGRAPHY

In this thesis diamond is used as an imprint lithography mold material, therefore the basics of imprint lithography and the use of diamond as imprint lithography mold material will be discussed in this Section. Imprint lithography is a high resolution, high throughput patterning method and was first reported by Chou et al. in the mid 1990's [14–16]. In the imprint lithography process, a surface pattern of a stamp is replicated into a material by mechanical contact and three dimensional material displacement as can be seen in Figure 2.6. When the dimensions of the imprint are below 100 nm, the process is called Nanoimprint Lithography (NIL).

Since no etching step is involved in the imprint lithography process, imprint lithography is especially suited for patterning of materials where either no good etch or no good anisotropic etch is available. Imprint lithography has many forms such as Thermal imprint lithography, UV imprint lithography, Cold pressing. Since the experiments in this thesis are done using thermal imprint lithography, only this method will be explained further.

Figure 2.6: Schematic overview of the imprint lithography process.

2.2.1. THERMAL IMPRINT LITHOGRAPHY

Thermal imprint lithography is a form of imprint lithography, which is commonly used for imprinting into polymers. As the name already suggests, thermal imprint lithography is an imprint lithography process performed at elevated temperatures. Usually polymers are heated well above their glass transition temperature before pressing the mold. However, one should be aware that too low viscosities enhance the danger of capillary bridges [17]. These capillary bridges decrease the imprint quality, mostly when imprint depth is below 80 nm [18]. When the mold is pressed into the substrate the polymer is gradually cooled down to below the glass transition temperature after which the mold can be released. A little over two decades ago in 1995 it was already possible to imprint sub 25 nm dots of 100 nm deep into PMMA [14]. Very soon thereafter, similar 25 nm features

with uniformity over a 15 x 18 mm^2 area imprint were demonstrated, furthermore 30 nm wide trenches with a depth of 70 nm were imprinted into PMMA [15].

2.2.2. DIAMOND IMPRINT LITHOGRAPHY

Diamond has first been used in 2000 as a mold material for imprint lithography of PMMA. Since then research has focused on imprinting higher aspect ratios, smaller structures and harder materials such as metals. However, the methods used for production of these diamond imprint lithography molds have only seen minor changes. In this Section the state of the art of diamond imprint lithography research, and the standard mold fabrication techniques will be discussed.

STATE OF THE ART OF DIAMOND IMPRINT LITHOGRAPHY

In this paragraph, a brief overview of the research on diamond imprint lithography that has already been reported in scientific literature will be presented. An important distinction between the work done in this thesis and the work already done by others is the way the diamond mold is fabricated. The standard way of producing diamond imprint lithography molds is by growing a relatively thick diamond layer, polishing this layer and then patterning the flattened diamond surface, which is schematically shown in 2.7. While this method gives a smooth diamond mold, it takes a lot of time since diamond is typically grown at rates of 1 μm/h, and patterning of diamond molds is an extensive and difficult process. Common microwave plasma-assisted etch rates are in the range of 5-7 μm/h, etch rates of up to 26.6 μm/h have been reported, increase of the etch rate leads to a lower selectivity and a decreased surface quality [19, 20].

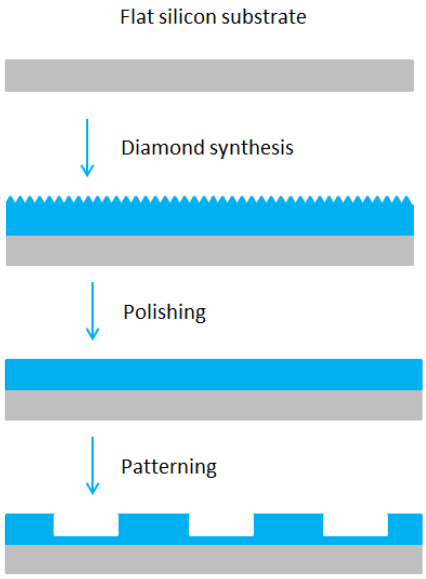

Figure 2.7: Diamond mold production method currently used in literature.

Diamond imprint lithography has until now mainly focused on imprinting into polymers, but there are also a few occasions where researchers report imprinting into glass materials or metals. In 2000, the first article appeared of successful imprinting using a diamond mold [21]. In this study, synthetic single-crystal diamonds were patterned using oxygen ion beam etching. Convex line patterns with a width of 600 nm and a depth of 150 nm, and convex line patterns with a width of 1100 nm and a depth of 180 nm were imprinted into PMMA. However, the quality of the PMMA lines was not very good since they showed evident asymmetry and additional roughness. Shortly thereafter, the same group did similar experiments. Again, synthetic single-crystal diamonds were used, but now patterning was done using RIE. This time, they were able to transfer 2 μm wide lines with a depth of 200 nm into PMMA with much more precision and accuracy than was the case in their previous attempts [22]. Furthermore, they also succeeded at imprinting into metals, a 1 μm wide line was transferred 100 nm into aluminum and 50 nm into copper.

Following, it was shown that it is possible to imprint with molds that have an aspect ratio of 10 (100 nm wide and 1 μm deep) [23]. This mold was fabricated by patterning CVD diamond through an ECR etch. In order to achieve this high aspect ratio a fluorocarbon monolayer was coated onto the mould to avoid sticking. Analysis of the imprinted PMMA, displayed in Figure 2.8, showed that an aspect ratio of over 20 (80 nm wide and 1780 nm deep) was attained while imprinting with the 100 nm wide and 1 μm deep mold. The difference between the size of the mold and the imprint is likely to be an effect of the stretching of the polymer when releasing the mold. The aspect ratio of 20 was thus attained by a mix of mechanical deformation and imprinting and not pure imprinting. In Figure 2.8, SEM images of the imprint results of Hirai et al are shown, imprints were done into PMMA. As can be seen in the Figure, the quality of the imprint gets worse with decreasing line width and the polymer stretching gets more pronounced.

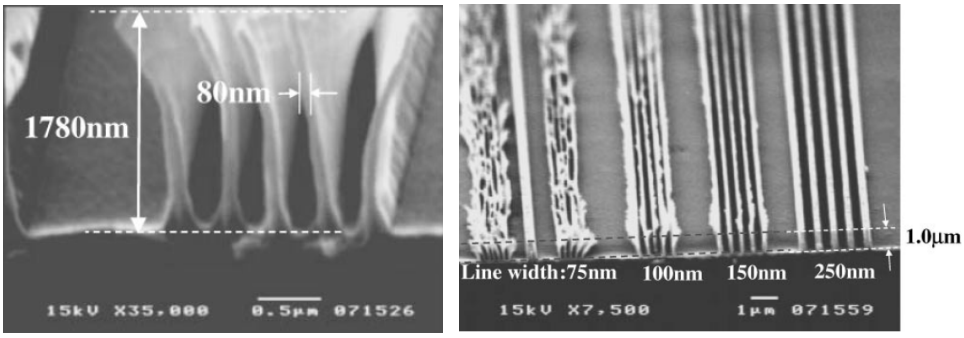

(a) Aspect ratio 20 imprint.

(b) Imprints of different dimensions into PMMA.

Figure 2.8: Diamond imprint results of Hirai et al. Reproduced from [23].

Up until 2008, no studies comparing the imprinting quality of diamond molds to molds fabricated out of other materials had been published. Papers only showed the ability to imprint with diamond molds but not the added value of using diamond for imprinting. In 2008, Komori et al. for the first time published a study in which a CVD diamond mold produced by FIB etching was compared to molds made out of silicon, glassy carbon, sintered CrN and sintered TiN [24]. Imprinting was done into pyrex, TEMPAX and BK7. The researchers needed sufficient strength at high temperatures (over 500°C) and high pressures in the molding process. Furthermore, a low adhesion between the mold and the imprinted materials is desirable for imprint lithography. They showed that the diamond mold was the only mold to not adhere to any of the imprint glass materials after imprinting in a wide range of temperatures, while all the other molds adhered to one or more of the materials inside the temperature range. Results are summarized in Table 2.1.

Table 2.1: Imprint test results of Komori et al. Reproduced from [24].

Candidate mold material	Glass	Molding temperature (°C)	Adhesion
(a) Under vacuum			
CVD diamond	Pyrex	580–690	No adhesion
	TEMPAX	565–640	No adhesion
	BK7	580–650	No adhesion
Silicon	Pyrex	580–650	Adhered
	TEMPAX	565–640	Adhered
	BK7	580–650	Adhered
Glassy carbon	Pyrex	650	No adhesion
		670–690	Adhered
	TEMPAX	565–615	No adhesion
	BK7	580–600	No adhesion
Sintered CrN	Pyrex	580–650	Adhered
	TEMPAX	565–590	No adhesion
		615	Adhered
	BK7	580	No adhesion
		600	Adhered
Sintered TiN	Pyrex	580	No adhesion
		600	Adhered
	TEMPAX	565–615	No adhesion
		640	Adhered
	BK7	580–600	No adhesion
		625	Adhered
(b) In nitrogen atmosphere			
Sintered CrN	Pyrex	580–650	No adhesion

CVD diamond also proved to be suited for imprinting into titanium, features of 200 nm with an aspect ratio of about 1 were transfered into titanium using an UNCD mold [25]. The UNCD mold was fabricated by patterning a 1.85 μm thick UNCD layer through the use of an oxygen based RIE etch. The researchers found that stamp features should have 20% additional height compared to the desired imprint depth, this additional height was needed to prevent the mold from breaking. The additional height prevents the bottom of the structures of coming into contact with the titanium, since full contact would result in a cracked substrate due to the applied pressure.

3

MOLD PRODUCTION METHODS

Silicon is at the moment a frequently used material to fabricate imprint stamps. Silicon stamps are relatively easy to fabricate, are cleanroom compatible, can withstand high temperatures, have a thermal conductivity of 149 W/m·K (at 25°C), and have a hardness of 13 GPa [26]. Lifetime of silicon imprint stamps is reported to be from tens of imprints to a few thousand imprints [17, 27]. For other mold materials such as PDMS approximately 20 imprints with the same mold are reported [28]. A reason for the big variation in lifetime of the silicon molds could be the desired surface quality, as well as the size of the imprint dimensions, and the desired imprint precision and accuracy.

Replacing these stamps with either a diamond coated micro-structured silicon mold, or a full diamond mold could significantly increase hardness, and wear resistance. Furthermore, the low thermal expansion coefficient of diamond will give better control over the dimensions of the structures when imprinting at elevated temperatures. The high thermal conductivity will ensure that heat spreads evenly throughout the mold, preventing unnecessary stresses to be induced. Unfortunately, production of diamond imprint molds is still a time consuming and expensive process.

In this Section the new methods for producing CVD diamond imprint molds will be explained. The focus of these methods is to drastically reduce the time, complexity, and costs involved in fabrication of such molds. This will be done by implementing two bottom-up approaches of creating diamond CVD molds instead of the usual top down approach as schematically shown in Figure 2.7.

Method 1 makes use of micro-structured silicon to grow diamond on, which means the time needed to grow diamond is much shorter, because only a thin layer has to be grown. Furthermore, no patterning step is needed after diamond growth. Method 2 can be used to grow patterned full CVD diamond molds by growing through porous templates. This means no further processing steps to pattern the diamond are needed after growth. Full diamond structures can thus be grown on wafer scale. For both methods single crystal, mirror polished <100> silicon is used as substrate. Silicon is very suited to grow diamond on because it is monocrystalline, resistant to high temperatures, cleanroom compatible, and does not dissolve carbon.

3.1. METHOD 1 - CVD DIAMOND COATED MICRO-STRUCTURED SILICON

In the first method proposed to reduce time and costs required for the fabrication of durable imprint molds, a micro-structured silicon substrate is overgrown with a thin CVD diamond film. Since only a thin film of CVD diamond (sub-micron thickness) has to be deposited, diamond synthesis duration is significantly reduced. The four basic steps involved in this mold production process are schematically shown in Figure 3.1. All of these steps will be explained in detail in Section 4.1.

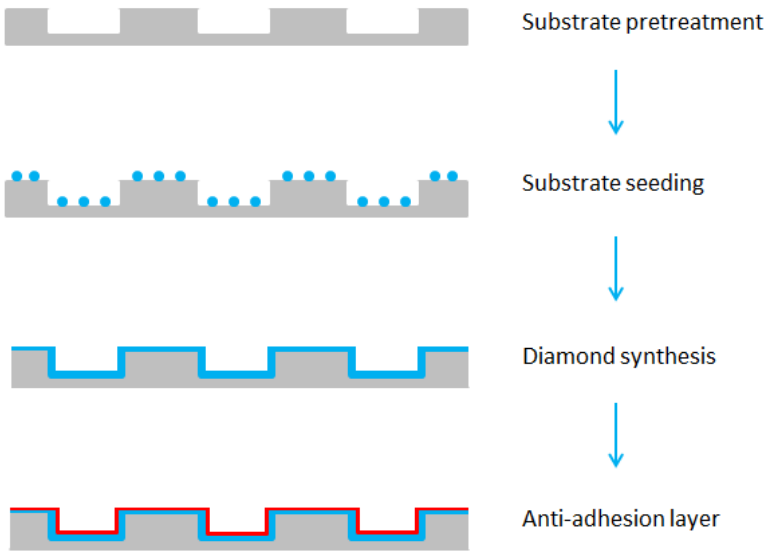

Figure 3.1: Overview of the fabrication of the diamond stamp according to Method 1.

3.2. METHOD 2 - TEMPLATE-GROWN CVD DIAMOND

The second method for the bottom-up production of CVD diamond molds is the so called template growth method. Because CVD diamond growth is limited to the areas where diamond seeds are exposed to diamond growth conditions, an unseeded porous template can be used to prevent diamond synthesis in certain localized areas. This obstruction will lead to the growth of structured diamond surfaces, which can be used as imprint mold. Thereby, no more polishing and patterning steps are required after diamond synthesis. A schematic overview of this method is given in Figure 3.2. All the steps involved in this fabrication process will be further discussed in Section 4.2.

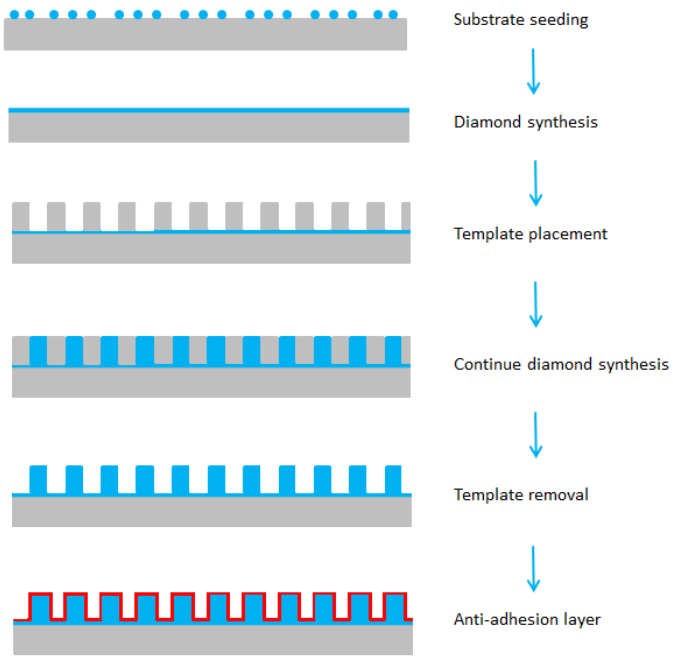

Figure 3.2: Overview of the template-grown diamond stamp according to Method 2.

3.3. ANTI-ADHESION LAYERS

Preliminary experiments, results of which can be found in Section 5.3.1, showed that imprinting the diamond layer without any post treatment was not always possible. Therefore, a way had to be found to reduce adhesion of the polymer to the stamp. In order to reduce the adhesion, anti-adhesion coatings will be investigated. FDTS has been identified as a promising candidate, this surfactant molecule contains fluor groups to reduce the surface energy of the stamp.

4

EXPERIMENTS

In this Section, methodology of the experiments will be discussed in detail. Details about the techniques employed for the fabrication and characterization of the samples are given in Appendix A.

4.1. METHOD 1 - CVD DIAMOND COATED MICRO-STRUCTURED SILICON

In this method the patterns on the micro-structured silicon substrate determines the final structure of the mold and is therefore very important. Five different kinds of micro-structured silicon substrates have been used, and an overview of the structures on these substrates can be seen in Table 4.1. Further information about the exact structures present on the surface can be found in Appendix B.

Table 4.1: Feature sizes of all dies.

Name	Trenches	Chessboard squares	Free standing squares	Circles	Depth	Die dimensions
Deep fully patterned	-	-	45x45 μm	-	47 μm	10x10 mm
Deep half patterned	-	50x50 μm	-	-	47 μm	10x10 mm
Shallow fully patterned	-	50x50 μm	-	-	500 nm	10x10 mm
Shallow half patterned	-	50x50 μm	-	-	500 nm	10x10 mm
Multi-patterned	1-100 μm	8x8 μm - 47x47 μm	5x5 μm - 49x49 μm	1.6 - 5 μm	350 nm	10x 5 mm

Deep and shallow structures have been chosen in order to be able to study the effect of aspect ratio on the imprint. Furthermore, both deep and shallow patterned substrates have a half and a fully patterned version. Whenever release of a half patterned mold is unsuccessful, one can quickly observe if the anti-adhesion layer, the patterns or both are the issue. When the unpatterned side releases but the patterned side does not, it is likely that this type of pattern is unsuited for imprinting. While the non-release of the entire stamp would lead one to suspect that the anti-adhesion layer is unsuited or not properly

applied. Finally, a multi-patterned substrate is used in order to be able to test a wide range of structure dimensions and aspect ratios in one imprint trial.

4.1.1. SUBSTRATE PRETREATMENT

Usually silicon is suited for seeding of the substrate without any pretreatment. However, it can be that due to the etching process or other treatment of the substrate, direct seeding proves unsuccessful. Initial seeding trials showed that the micro-structured silicon substrates are far from suited for direct seeding, meaning they have to be pretreated. Seeding results can be found in Section 5.1. The goal of this pretreatment is to make the top layer of the surface of the sample negatively charged, as will be further explained in Section 4.1.2. One of the ways to make the surface charge negative is to terminate it with oxygen, which can be done via several methods. Exposure to both oxygen plasma and acid treatment have been investigated (details can be found in Appendix A.2).

4.1.2. SUBSTRATE SEEDING

Once the sample is pre-treated, it is ready to be seeded. Diamond seeding is necessary since initial nucleation of diamond during the CVD process requires a lot of energy, and results in poor surface coverage. Dense seeding is very important, since it determines the minimum layer thickness needed to grow a closed diamond layer. The larger the distance between the seeds, the thicker the layer has to be in order to be closed. Furthermore, a densely seeded substrate will generally result in smaller diamond crystals at the surface and therefore less surface roughness. Seeding is done using very small diamond particles dispersed in a solution. The mother solution used for seeding in this thesis is NanoAmando, whose properties can be found in Table 4.2. This mother solution is diluted in ethanol to get a diamond nanoparticles solution with a concentration of 2 g/L.

Table 4.2: Properties of NanoAmando solution.

Product	1st particle size (nm)	Abundance (%)	2nd particle size (nm)	Abundance (%)	ζ-potential (mV)
NanoAmando	5 ± 1	99 ± 1	48 ± 14	1 ± 1	+49.2 ± 0.4

Important for a good seeding solution are the abundance of small particles (around 5 nm) and the ζ-potential of the solution. The seeds attach to the substrate through Van der Waals forces. Therefore, smaller particles will stick better to the surface than bigger particles due to the higher surface-to-volume ratio. Small particles are also required to attain very dense seeding. However, these small particles tend to form agglomerates if no precautions are taken to prevent this. By adjusting the ζ-potential the agglomerate formation within the solution can be prevented. A colloidal solution is considered stable when the value of the ζ-potential is either above +30 mV or below -30 mV [29]. The NanoAmando solution has a ζ-potential of +49 mV, and is therefore considered stable. A positive ζ-potential is an effect of H-termination of the diamond nanoparticle surface. Because the ζ-potential of the diamond nanoparticles is positive, a negatively charged substrate surface is required. In order to prevent repelling of the diamond seeds and thus

promote a high seeding density on the surface. Seeding is done by following the protocol described in Appendix A.2.

4.1.3. DIAMOND THIN FILM SYNTHESIS

Once dense seeding is obtained the growth process can be started. The samples used for imprinting are overgrown with a diamond layer of approximately 0.5 μm. The thin film is grown to 0.5 μm to ensure a closed layer, and strong interconnection of the layer. Growing thicker than 0.5 μm would lead to a larger surface roughness, a loss of structure definition, increase in structure dimensions, and additional growth time, and therefore growth is limited to 0.5 μm. The diamond synthesis protocol, and the equipment used can be found in Appendix A.2.

4.2. METHOD 2 - TEMPLATE-GROWN CVD DIAMOND

The second mold production method investigated in this thesis depends on the confinement of diamond growth to certain directions. The protocol for fabrication of these molds will be explained in this Section.

4.2.1. SUBSTRATE PRETREATMENT AND SEEDING

Since the silicon wafers used for template growth proved to be suited for direct seeding (results can be found in Section 5.1), no pretreatment is required. This is due to the fact that the surface of the silicon wafers is sufficiently negatively charged in order not to repel the diamond seeds. Seeding is done by following the protocol described in Appendix A.2.

4.2.2. DIAMOND SYNTHESIS

Diamond synthesis needs to be done in two steps for the template growth molds. In this section these two steps will be described and the reason for using two steps in stead of one will be explained. The diamond synthesis protocol, and the equipment used can be found in Appendix A.2.

FLAT THIN FILM SYNTHESIS

There are several reasons to synthesize a flat thin layer before starting the synthesis of the structures. The flat diamond layer protects the parts of the silicon where no diamond structures will be synthesized on, and can also distribute the pressure over the silicon substrate during imprinting. The thickness of this layer can thus be varied with the hardness of the imprint material. Because imprints in this thesis will be done into polymers, only a thin film of diamond is needed, and therefore the thin film synthesis is limited to 0.5 μm.

Apart from this, the layer of diamond seeds is very frail as discussed in Appendix A.2. Because the diamond seeding layer is so frail, it is not possible to manually place a template without damaging it. In order to avoid this problem a thin diamond film is grown. Placing a template on this thin diamond film can be done manually without resulting in any damage.

PATTERN SYNTHESIS

After synthesis of the flat diamond layer, patterns can be synthesized. Pattern synthesis is done through porous silicon templates fabricated by Smart Membranes. The template used contains square pores of 2.5 μm x 2.5 μm on the bottom side, spaced 4.2 μm apart and order hexagonally. The template has a thickness of 17.5 μm. An image of the bottom of the template can be seen in Figure 4.1. Also displayed in Figure 4.1 is a side view image of a porous silicon template (placed upside down) that has been cut in pieces. The structure of the holes in the top (bottom side in Figure 4.1) of the template is not relevant for the shape of the diamond patterns near the bottom (top side in Figure 4.1) of the template and can thus be an arbitrary shape. However, these holes should be as large as possible to allow the best growth conditions near the diamond surface.

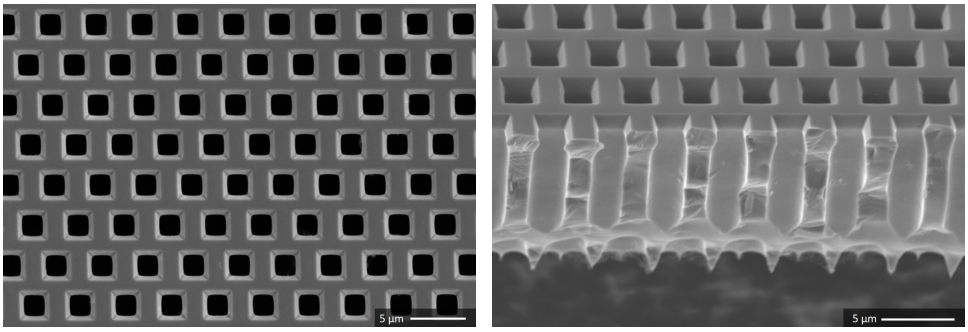

(a) Bottom side of the porous silicon template. (b) Side view of the porous silicon template.

Figure 4.1: SEM image of the porous silicon template.

As is visible in the images above, the first part from the top has a well defined pyramid-like structure which is likely to be easy to release. However, further down the template the pores get wider again, meaning the template and thus also the imprint cannot be released when diamond is grown too far beyond the pyramid-like structure.

The template is manually placed on top of the thin diamond film. Since the template is extremely thin and therefore light, it had to be mechanically fixed to the diamond layer underneath. After the template is placed, the diamond synthesis can continue. In this way, the diamond layer grows through the pores in the template and will not grow further in the areas covered by the template. The shape and size of the patterns grown are therefore determined by the shape and size of the holes in the template (different types of structures could be synthesized with other porous templates).

4.2.3. TEMPLATE REMOVAL

When the template growth is finished, the template has to be removed. Two methods have been explored to remove the template: ultrasonicating in Acetone and KOH etching. Which method is preferred depends on the height of the pillars and thereby on the growth duration. If the pillars get higher than about 1.5 μm, the template will be locked by the diamond pillars and it will be impossible to remove the template by ultrasonicat-

ing, so the template has to be etched off.

ULTRASONICATION IN ACETONE

As mentioned earlier, the template can be ultrasonicated of when the pillars have not yet locked the template to the substrate. This method should make it possible to remove the template without destroying it. If the pillars are small enough, the template is expected to come off in one piece within a few minutes of ultrasonication. In theory, the template should be reusable after removal from the mold.

KOH ETCHING

When structures have been grown to a height which will lead to mechanical interlocking of the template, ultrasonication of the mold in Acetone is unlikely to remove the template. The mold then has to be removed by chemical etching in KOH. But first, the sample is treated with acids as explained in Appendix A.2. This is done to make sure there is no sp^2 carbon content (deposited by the HFCVD process) left on the template that could protect it from the KOH etch.

The KOH solution used to etch the template contains 40 gram KOH, which is mixed with 100 ml of DI water. The resulting KOH solution has a concentration of 7 mol/L. This solution is then heated to the boiling point, and the sample is submerged in it until the template is removed.

4.3. ANTI-ADHESION LAYERS

In order to reduce the surface energy of the diamond layer, and thereby make release of the mold from the polymer easier, anti-adhesion layers have been investigated and will be discussed in this Section. A low surface energy means that the material repels adhesives which is particularly important for imprinting molten materials where otherwise chemical reactions may cause diffusion and bonding of ions at the interface [30]. Results regarding the coating and surface modification of these anti-adhesion layers can be found in Section 5.3.

4.3.1. PERFLUORODECYLTRICHOLOSILANE (FDTS)

The most promising of the anti-adhesion layers explored was perfluorodecyltrichlorosilane (FDTS), shown in Figure 4.2. This surfactant molecule contains fluor groups to reduce the surface energy of the stamp.

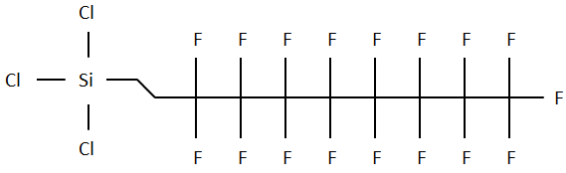

Figure 4.2: Molecular structure of FDTS.

This anti-adhesion layer is able to form covalent bonds with -OH groups at the surface of the diamond film [31]. The availability of -OH groups at the surface is ensured by using the same acid treatment as is used before the seeding, which can be found in Appendix A.2. When exposed to DI water after acid treatment, -OH groups will form at the surface. If these -OH groups are exposed to the FDTS, covalent bonds are formed as is shown in Figure 4.3. These bonds enable deposition of a monolayer of anti-adhesion coating on top of the diamond film.

Two methods of depositing FDTS have been explored, vapor coating of FDTS and dispersion of the molds in a FDTS solution. The methods have been compared by measuring the contact angle with water. Results of this study including the optimized coating protocol are presented in Section 5.3.

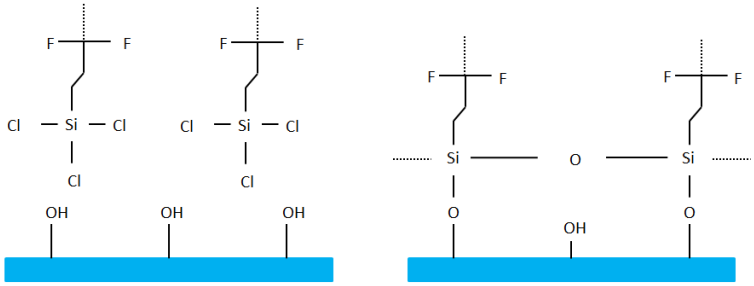

Figure 4.3: Reaction of FDTS with -OH groups at the surface.

4.4. IMPRINT EXPERIMENTS

In order to verify suitability of the molds for imprint lithography, imprint experiments have been done. Initial trials have been done by casting PDMS, since it is a relatively soft polymer. Further validation was done by imprinting into polymers above their glass transition temperature. This is the so called thermal imprint lithography process. An overview of the system used for the imprint experiments can be found in Appendix A.3.

4.4.1. PDMS SOFT EMBOSSING

In order to check if imprinting into a soft polymer (before moving to the harder polymers used for thermal imprint lithography) was possible, an imprint into PDMS has been done. Details of the PDMS casting protocol can be found in Appendix A.3.3.

4.4.2. THERMAL IMPRINT MATERIAL

As imprint material cyclic olefin copolymer (COC), developed by TOPAS Advanced Polymers has been chosen. This material will be referred to as COC hereafter. Two different types of COC wafers will be used. The first is a 300 μm thick TOPAS®COC wafer grade 8007, with a glass transition temperature of 70°C. The second is a 1 mm thick TOPAS®COC wafer grade 6013, with a glass transition temperature of 130°C. Among the reasons for choosing to imprint a COC are high chemical resistance, low water absorption, good optical transparency, large Abbe number, and low birefringence. An overview

of TOPAS® COC properties is presented in Appendix G. These properties make COC suited for a wide range of applications such as, microfluidic devices, micro optical components, and electrochemical sensing [32, 33].

4.4.3. EXPERIMENTAL PLAN AND IMPRINT PARAMETERS FOR THERMAL IMPRINT LITHOGRAPHY

After both methods for the fabrication of the diamond imprint stamps have been established, including the specific type and procedure for coating the anti-adhesion layer, the suitability of the molds for thermal imprint lithography can be validated. In order to do this validation the correct imprint parameters have to be found. Parameters that will be varied in this study are: imprint pressure, imprint temperature, and possibly imprint duration. Temperature will be varied in steps of 20 °C, starting from the glass transition temperature up until a full imprint is realized. Increasing the temperature further would lead to a even higher viscosity, which leads to pressing the polymer away instead of imprinting. The pressure will be 30 MPa in the initial experiment, which will be decreased if the mold is embedded too far into the polymer. Embedding of the mold far into the polymer could make release of the mold harder. The pressure will be increased if the micro-structures on the mold are not fully transfered. The imprint duration will be 8 minutes in the initial experiment and will only be increased if necessary.

Once the right imprint conditions for each sample are established, the experiments will be replicated for both the diamond-coated and the template-grown molds.

5

RESULTS & DISCUSSION

In this Section, the experimental results will be discussed. First, a few preliminary experiments will be discussed, then the anti-adhesion layers, and finally the results of the mold production and imprint.

5.1. SEEDING DENSITY

Of the two methods explored in an attempt to improve seeding on the micro-structured silicon substrates, acid treatment proved to be the most effective. The use of the oxygen plasma procedure, explained in Appendix A.2, showed very little improvement compared to an untreated micro-structured silicon substrate. Therefore, the micro-structured silicon substrates treated with oxygen plasma have not been further analyzed.

In order to be able to quantify the coverage of the seeding, the SEM images of seeded substrates have been analyzed using ImageJ. Using this software, the percentage of the total area covered by agglomerates of seeds can be determined, as well as the number of agglomerates, and the average size of the agglomerates in nm^2, as seen from top view. Figure 5.1 shows the original SEM images of the seeding together with the particle analysis images produced by ImageJ.

As is also clearly visible on the images, seeding coverage of the untreated micro-structured silicon samples is very poor. In the image, 7 agglomerates of an average size of 584 nm^2 are visible, which results in a surface coverage of 0.1% and in a seeding density of 2.24×10^8 agglomerates/cm^2. If these values and the images are compared to seeding of a standard single crystal, mirror polished <100> silicon piece, the difference is significant. Standard seeded silicon has 525 agglomerates on the same area with an average size of 950 nm^2, resulting in a seeding density of 1.85×10^{10} agglomerates/cm^2 and 17.6% surface coverage. When analyzing the seeding of a micro-structured and then acid treated silicon sample, it can be seen that seeding has improved drastically. Now 692 agglomerates are present on the same area averaging 459 nm^2 in size, leading to a surface coverage of 11% and 2.47×10^{10} agglomerates/cm^2. An overview of the seeding analysis data can be found in Table 5.1.

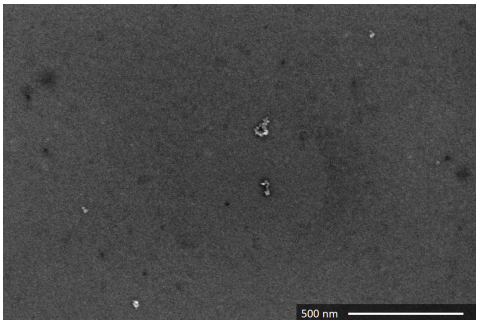

(a) Untreated micro-structured seeding.

(b) Untreated micro-structured analysis.

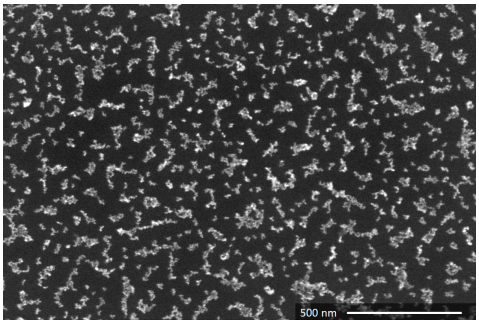

(c) Standard silicon seeding.

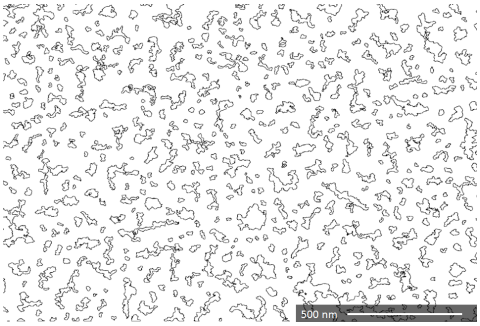

(d) Standard silicon analysis.

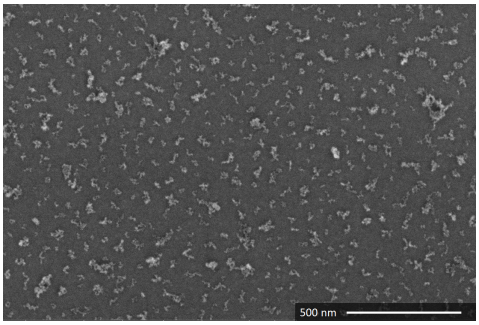

(e) Seeding of acid treated sample.

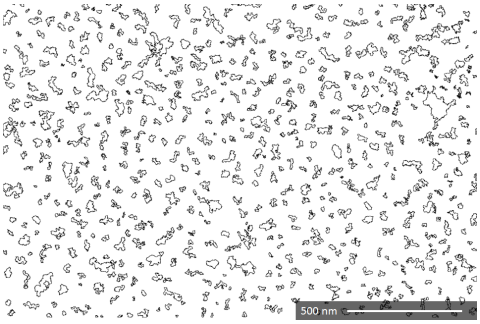

(f) Analysis of acid treated sample.

Figure 5.1: SEM images of the seeding (left). and ImageJ analysis of these images (right).

Table 5.1: Seeding data of all the samples.

Sample	Number of agglomerates	Average size (nm^2)	Coverage (%)	Agglomerates/cm^2
Untreated micro-structured silicon	7	584	0.1	2.24×10^8
Standard silicon	525	950	17.6	1.85×10^{10}
Acid treated silicon	692	459	11.3	2.47×10^{10}

The seeding density attained in this thesis is slightly better than the seeding density of 1.4×10^{10} agglomerates/cm^2 reached by Tsigkourakos et al. [34].

From the preceding table and images, it can be concluded that acid treatment of the etched samples before seeding is necessary. Without acid treatment, the seeding is not dense enough to be able to grow a thin closed diamond film.

The standard silicon seeding has a higher % area coverage and larger agglomerates but a lower number of agglomerates/cm^2. Ideally one would want a high % of the area covered in agglomerates that are as small as possible and attain equal spacing between the agglomerates. Despite the lower coverage that it produces, the acid treatment before seeding seems to be better suited for diamond growth due to the smaller agglomerate size and the larger number of agglomerates/cm^2. Additional SEM images of seeded substrates can be found in Appendix E.

5.2. RESULTS OF SOFT EMBOSSING INTO PDMS

Soft embossing into PDMS (protocol described in Appendix A.3.3) has been done using a shallow half patterned mold. The shallow half patterned silicon substrate was overgrown with 0.5 μm of CVD diamond. No anti-adhesion layer was required for soft embossing into PDMS. Images of the mold and the PDMS imprint are presented in Figure 5.2. As can be seen in this Figure, the imprint into PDMS matches the dimensions of the mold very well.

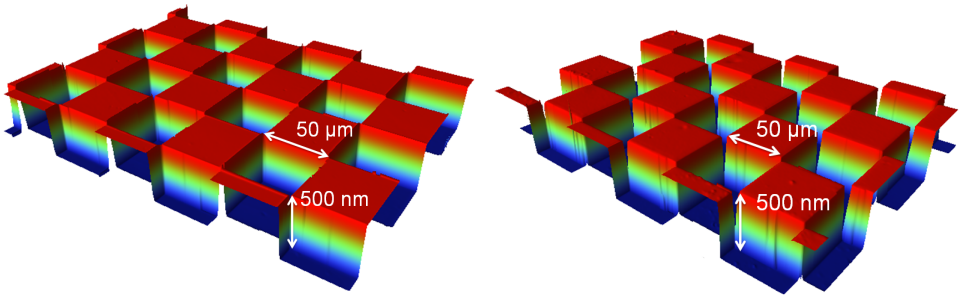

(a) CVD diamond coated silicon mold. (b) Imprint into PDMS.

Figure 5.2: PDMS experiment, images made with a white light interferometer.

In order to be able to get a better indication of the quality of the PDMS imprint, the line profiles of both 3D optical microscopy images have been compared. This comparison can be found in Figure 5.3, the line profile of the PDMS imprint has been rotated 180° around the x-axis. As can be seen in Figure 5.3, the line profile of the PDMS imprint matches the line profile of the diamond mold quite well.

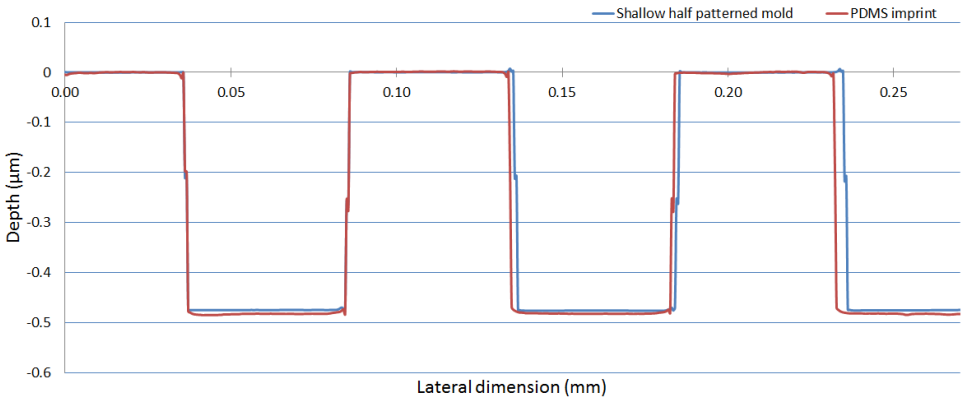

Figure 5.3: Line profiles obtained with a WLI, PDMS imprint profile has been rotated 180° around the x-axis.

The lateral dimensions of the PDMS imprint are slightly smaller as can be seen in the increasing gap between the imprint and the mold line profiles. The most likely reason for this difference is the larger contraction of the PDMS when temperature decreases. The PDMS will contract after soft embossing because it is cured at 70 °C and further inspected at room temperature. Since the thermal expansion coefficient of PDMS ($3 \cdot 10^{-4}$/°C) is about 100 times larger than that of silicon ($2.6 \cdot 10^{-6}$/°C), the shrinkage of the PDMS imprint will be much larger [35]. This effect will likely also cause a small difference in the height of the structures. Since the results of imprinting into PDMS were good, further research has focused on imprinting into COC.

5.3. CVD DIAMOND ADHESION & ANTI-ADHESION LAYER

5.3.1. UNTREATED CVD DIAMOND AS IMPRINT MATERIAL

An experiment was conducted in order to verify if CVD diamond (grown at standard conditions) without any post treatment was suited for imprinting into the harder COC. In order to verify this, a flat piece of silicon wafer was overgrown with 0.5 μm diamond and imprinted into TOPAS®COC grade 8007, which has a glass transition temperature of 70 °C. The imprint was done at 110 °C, with a pressure of 8 MPa for a duration of 8 minutes. This test proved to be unsuccessful, as can be seen in Figure 5.4. When trying to release the imprint mold from the polymer, the diamond layer partially broke off from the silicon substrate. This indicates that adhesion between the CVD diamond layer and the polymer is too high, at certain areas even higher than the adhesion of the diamond layer to the silicon substrate.

Another experiment in which a multipattern diamond mold was used for imprinting into COC was successful. Imprinting was done into TOPAS®COC grade 6013 at 170 °C, 10 MPa, 8 min imprint duration. While this imprint experiment was successful, release of the mold was very difficult and involved quite some bending of the polymer.

Due to the mixed results of imprinting with an untreated CVD diamond layer, and the difficulties with the release of the mold, further experiments were done with molds coated with an anti-adhesion layer.

5.3.2. FDTS

A new protocol for deposition of FDTS has been developed. First, vapor deposition and dispersion deposition have been compared in order to determine the general deposition mechanism. Comparison was done by determining wettability of samples coated through vapor or dispersion deposition. These measurements have been done with a OneAttension Theta Optical Tensiometer. Contact angle measurements on an as-grown CVD diamond layer resulted in a contact angle of 80^o with DI water. Vapor deposition of FDTS resulted in a contact angle of 30^o, while dispersion deposition resulted in a contact angle of 95^o. The decrease in the contact angle when FDTS was coated with vapor deposition can be attributed to the acid treatment. Termination of the surface with oxygen leads to a hydrophilic surface and thus a decrease in contact angle. When a anti-adhesion layer is not properly deposited afterwards, the contact angle will be lower than the contact angle of as-grown CVD diamond. Due to the significantly better results with dispersion deposition, this type of deposition is further optimized.

The optimized FDTS dispersion coating protocol is shown below:

1. Dilute FDTS in ethanol with a 1% weight percentage of FDTS.
2. Ultrasonicate for 10 minutes to make sure FDTS is fully diluted.
3. Submerge samples in the solution, ultrasonicate for 30 seconds, expose sample to solution for 30 minutes.
4. Ultrasonicate sample in ethanol for 30 seconds.
5. Bake samples at 130 °C for 30 minutes.

The ultrasonication step after submerging the samples in the FDTS solution is added in order to attempt to get rid of air bubbles that might be stuck in the bottom of the structures. Ultrasonication in ethanol after the sample is taken out of the solution is done to get rid of large quantities of FDTS on the surface. Tests without this step showed surfaces with FDTS stains (so definitely no monolayer). The last bit of excess FDTS is removed by baking the sample.

In order to determine the effect of this anti-adhesion layer on the surface energy, the surface energy of the sample was determined before and after coating with FDTS. The FDTS coating resulted in a decrease in surface energy from 49 mN/m to 40 mN/m (calculated using the OWRK method). Full explanation and the results of these measurements can be found in Appendix D.2.

Furthermore, a quantitative experiment to test the release of a FDTS-coated CVD diamond layer has been done following the same procedure as in Section 5.3.1. The FDTS-coated CVD diamond layer released easily without any damage to the mold, as can be seen in Figure 5.4.

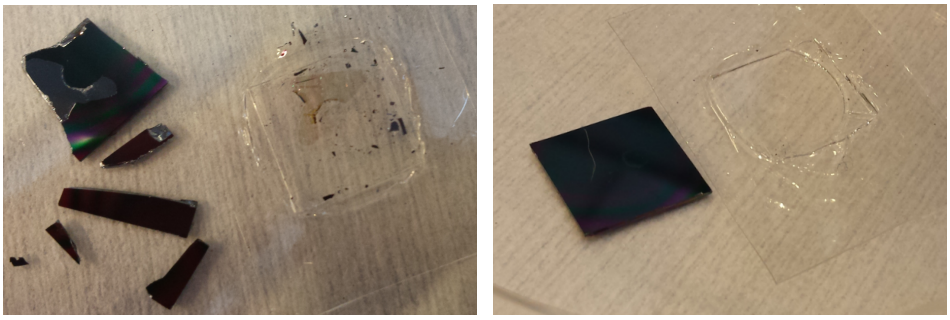

(a) Flat CVD diamond imprint. (b) Flat FDTS-coated CVD diamond imprint.

Figure 5.4: Comparison of flat CVD diamond layer imprint with and without anti-adhesion layer.

5.4. METHOD 1 - CVD DIAMOND COATED MICRO-STRUCTURED SILICON

5.4.1. MULTI-PATTERNED MOLD

MOLD PRODUCTION

In order to protect the silicon substrate underneath, it is very important that the diamond layer is closed and therefore no more silicon is exposed. High-resolution SEM images (Figure 5.5) have been made to verify that the diamond layer is closed. As can be seen in the images, the diamond layer is fully closed and no more silicon is exposed.

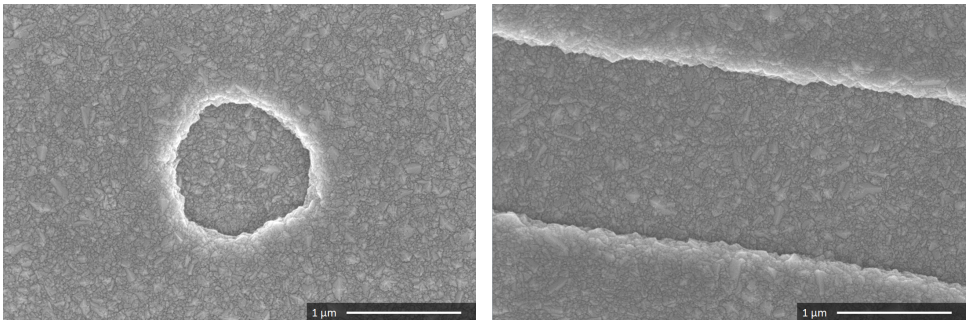

(a) Diamond overcoated hole. (b) Diamond overcoated trench.

Figure 5.5: SEM images of the diamond layer coated on the multi-patterned substrate.

A further SEM analysis was done in order to investigate the effect of the coating of a 0.5 μm diamond layer on the shape of the smallest, μm-sized, structures. These images are shown in Figure 5.6. As it was expected, the relative dimensions of the structures have increased significantly due to the 0.5 μm thick diamond coating. The uncoated silicon structure has a lateral length of 0.7 μm along the shortest side, which is increased to 1.5 μm when the diamond film is deposited. A change in the shape of the structure can also be observed, as the diamond coated structure has become a lot rounder.

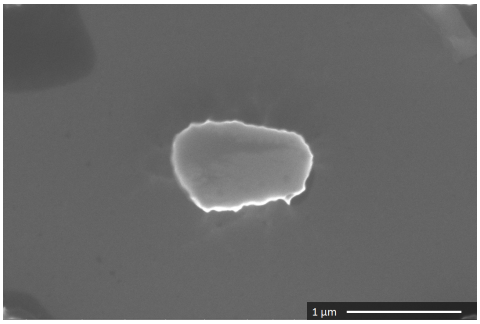

(a) Silicon structure.

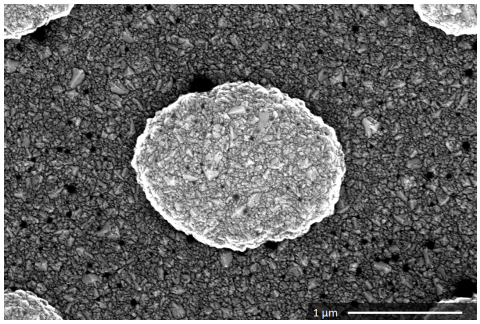

(b) Coated with 0.5 μm diamond.

Figure 5.6: SEM images of the smallest protruding structure on the multi-patterned mold, with and without diamond coating.

In Figure 5.7, a similar analysis of the influence of the diamond coating on the shape and dimensions of the structures has been performed. However, these images show depressions in the substrate instead of structures coming out of the substrate. Analysis shows that the diameter of the circular structure has decreased from 1.9 μm to 1.1 μm. Due to the changes observable in the shape and dimensions of structures after deposition of diamond, it is advisable to design the silicon substrate in a way that the desired structure dimensions are attained after diamond growth.

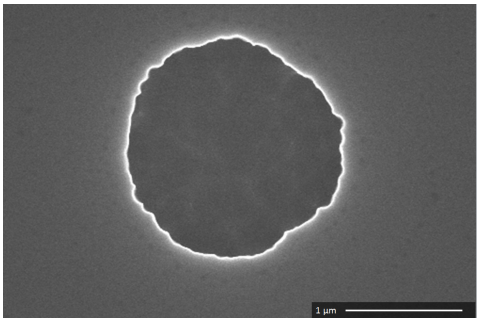

(a) Silicon structure.

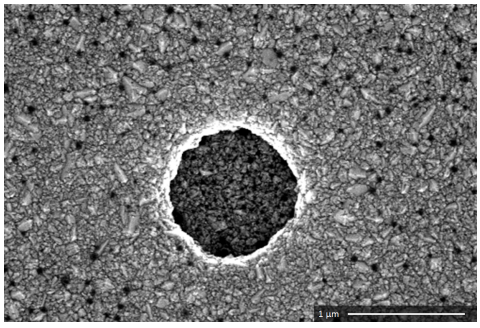

(b) Coated with 0.5 μm diamond.

Figure 5.7: SEM images of the smallest depressions in the multi-patterned mold, with and without diamond coating.

While the SEM images clearly show the presence of diamond on the surface, this had to be verified with Raman spectroscopy. Raman spectroscopy showed that there is diamond present on the surface. Full results of this analysis can be found in Appendix C.

IMPRINT INTO COC

Because preliminary experiments proved that the TOPAS®COC grade 8007 with a thickness of 300 μm was too thin, the TOPAS®COC 6013 with a thickness of 1 mm has been used for all following COC imprinting experiments. As mentioned in the experimental plan, the right parameters for imprint had to be found. Experiments done at 130 °C and 150 °C did not result in full imprints (meaning the pattern was not fully transfered), but imprinting at 170 °C resulted in proper transfer of the patterns. Imprint pressure was found to be optimal at 10 MPa, which was as high as possible without embedding the mold in the polymer too much. Pressing the mold deep into the polymer made release of the mold difficult and therefore increases the risk of breaking the mold when releasing it from the polymer. Release is done by slightly bending the polymer and then peal it of with a tweezer as is schematically shown in Figure 5.11. The imprint duration of 8 minutes proved to be sufficient for full pattern transfer and was therefore not increased.

A 3D optical microscopy image of one of the imprints done with the optimal parameters (170 °C, 10 MPa, 8 min) can be found in Figure 5.8. This image was corrected for measurement artifacts by applying a 2nd degree polynomial background subtraction along both directions.

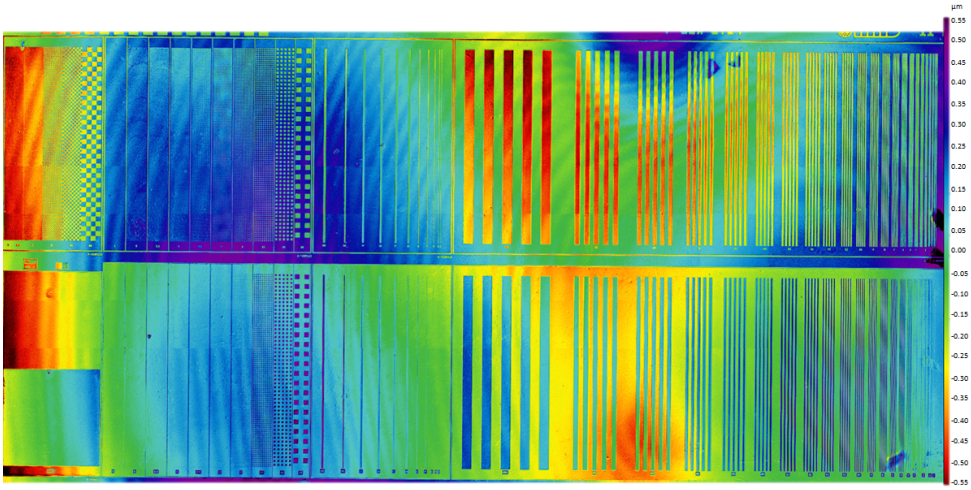

Figure 5.8: 3D optical microscopy image of the imprint of the diamond coated multi-patterned mold into COC.

As far as can be seen in the 3D optical microscopy overview image, the imprint seems to be a faithful replication of the mold. However, the polymer is not as flat as the mold throughout the imprinted area, which could be an effect of the release procedure. The image also shows some stains, these are defects in the mold that were transfered into the polymer as can be seen in Figure 5.9. The source of these defects remains unknown, but the defects were likely to be present in the silicon substrate or caused by problems with the diamond seeding layer.

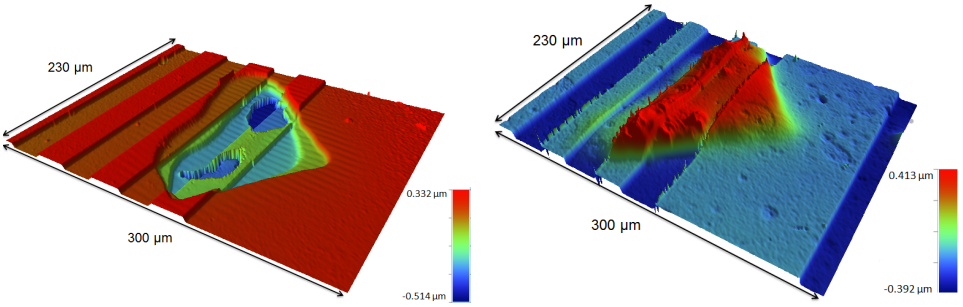

(a) Defect in the diamond mold.

(b) Defect transferred into COC imprint.

Figure 5.9: 3D optical microscopy images of a defect in the mold and in the imprint.

Further analysis is done with the SEM since the resolution of the whitelight interferometer is not good enough to be able to analyze the smallest structures. The images of the SEM analysis of the finer structures are shown in Figure 5.10.

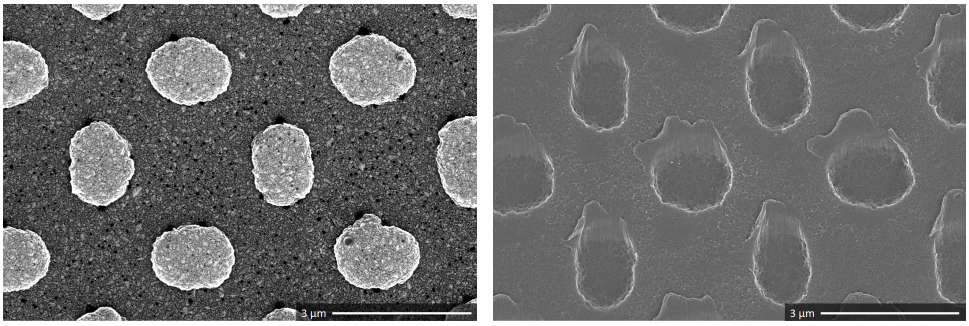

(a) Diamond mold.

(b) Imprint into COC.

Figure 5.10: SEM images of the mold and imprint into COC of the small structures on the multi-patterned mold.

The imprints are faithful replications of the mold as far as can be judged from these images, analysis along of lengths along the horizontal direction show that dimensions of the mold and imprint match exactly. However, some damage is visible on the imprint. This damage is likely to be caused by a shift of the mold during imprinting or during release. This kind of damage could be prevented by a better releasing procedure in which the mold is extracted from the polymer by strictly vertical translation as is schematically shown in Figure 5.11. Or by mounting the stamp to the thermal imprint setup, shifting of the mold during imprint is then no longer possible.

Despite the suboptimal release procedure, releasing the mold without breaking it was possible. Therefore, subsequent imprint experiments with the same mold could be conducted. The second imprint experiment with the same mold also resulted in accurate replication of the patterns.

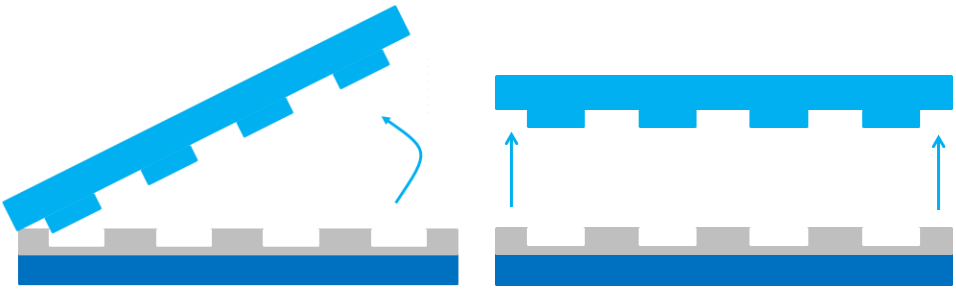

(a) Current approach. (b) New approach.

Figure 5.11: Current release procedure in which the mold is pealed from the polymer, and new release procedure where the mold is extracted strictly vertically from the polymer.

5.4.2. DEEP HALF & FULLY PATTERNED MOLD

MOLD PRODUCTION

The mold production of the deep half and fully patterned molds gave similar results to the production of the multi-patterned molds. The growth of 0.5 μm of CVD diamond also proved to be enough to form a closed layer on the deep substrates.

IMPRINT INTO COC

The imprints into COC with the deep molds were done following the experimental plan described in Section 4.4.3. The imprint pressure was found to be optimal around 10 MPa as was the case with the multipattern mold. The temperature was increased among consecutive experiments from 130 °C in steps of 20 °C. At 130 °C, a very shallow imprint of about 10 μm was realized (height was determined with the whitelight interferometer). When the temperature was increased to 150 °C the imprint reached a height of about 26 μm. Results of this imprint are shown in 5.12. The image clearly shows that the imprint has a round shape, and that some polymer was torn off at the sides. Since this is not yet a full imprint, the temperature was increased further to 170 °C. However, at this temperature, release of the mold was not possible.

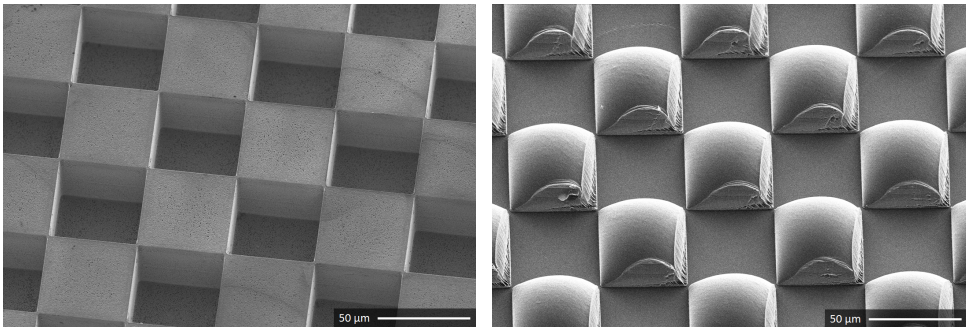

(a) Deep half patterned mold. (b) Imprint into COC.

Figure 5.12: Deep half patterned imprint into COC at 150 °C, images made with a SEM under 30°.

There are several possible reason for the inability to release the mold. First, the deep molds contained rugged sidewalls in the silicon substrate, as an effect of the fabrication by deep reactive ion etching, which are shown in Figure 5.13. These rugged sidewalls could interlock with the polymer during the imprint, and thereby make release much more difficult.

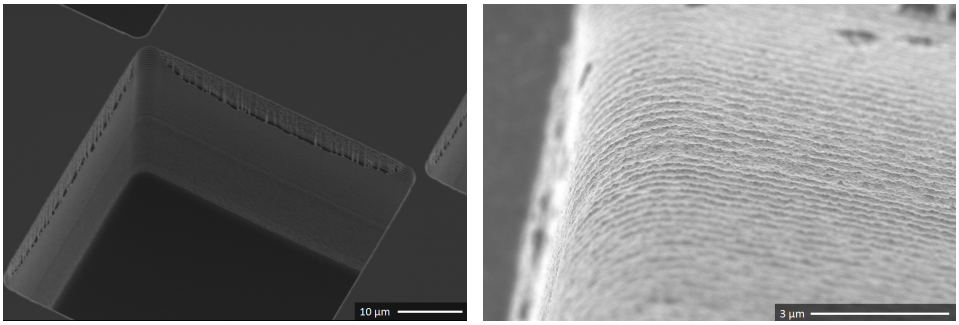

Figure 5.13: 30° SEM images of the rugged side walls of the deep diamond molds.

Another reason could be the layout of the substrate. Since the cubic structures are oriented as a checkerboard with closed corners, air cannot flow in during the release process and thus the imprint remains strongly attached to the mold due to vacuum.

5.5. METHOD 2 - TEMPLATE-GROWN CVD DIAMOND

5.5.1. MOLD PRODUCTION

Template-grown molds were produced as described in Section 4.2. The aim with this mold production process is to grow diamond structures up to the height where release of the mold after imprinting is still possible. That means growing up to a height of about 1.5-2 μm. Diamond has been grown far beyond the pyramid-like structure. The molds produced this way are not included in the results because they cannot be imprinted, but can be found in Appendix F. The duration of synthesis required to reach the height of about 1.5-2 μm is experimentally determined to be around 6 hours. Therefore, all stamps discussed in this Section contain structures synthesized for a total duration of 6 hours. This means that the porous silicon template severely reduces the diamond deposition rate, since the standard deposition rate is approximately 2 μm/h.

TEMPLATE REMOVAL

During the removal of the template from molds grown for 6 hours, it became clear that ultrasonicating in Acetone was not enough to remove the entire template, as the process removed small pieces of the template but did not remove the entire template. A partially removed template is shown in Figure 5.14. The right side displays diamond structures as grown through the template, the left side shows a piece of porous silicon template still stuck on the surface. This sample has been ultrasonicated in Acetone, but in some areas the structures grew high enough to lock the template.

When this happens, the template breaks off in the spots where it is not locked in, and a partially removed template is left over. The last pieces of template have to be etched away.

The KOH etch rate at boiling point, using the concentration indicated in Section 4.2.3, has been experimentally determined to be 330 μm/hour. However, etching of the template interlocked by the diamond proved to be a slower process than etching of a silicon wafer. Therefore about 15-20 minutes of exposure time to the KOH etch was required to remove the template. The reduced etching rate could be caused by the orientation of the crystal in the porous silicon template, because KOH etching of silicon is an anisotropic process [36]. Or could be an effect of a protective layer of sp^2 carbon (even after acid treatment).

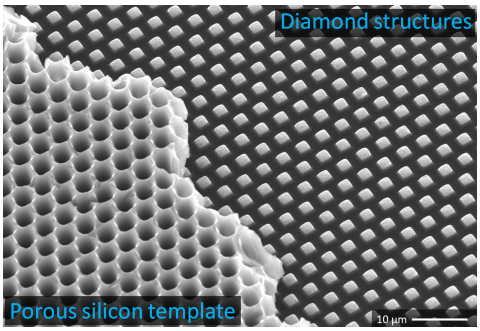

Figure 5.14: Partially removed template, 30° SEM image.

RESULTING DIAMOND STRUCTURES

The porous silicon template does not connect perfectly to the diamond film underneath. Due to its very small thickness, the template bows very easily which results in air gaps between template and diamond film. Because of the suboptimal connection of the template, variation of the height of the diamond structures throughout the mold is observable. Three main types of areas can be distinguished (also shown in Figure 5.15):

1. Areas where the porous template did not connect properly, and therefore no structures have been grown.

2. Areas of partially grown structures. A gradient in structure height is observable in these areas.

3. Areas of full grown structures, here the template connected well and the structures have been growing through the template for 6 hours.

Also visible in Figure 5.15 are some black dots or lines, these are spots where no diamond structures were synthesized. This is likely to be due to contamination with dirt, but no definitive conclusion can be drawn here.

The indicated areas have been studied more closely, and are shown in Figure 5.16. In area 1, a flat diamond layer is visible, which is quite uniform throughout the mold. Area 2 contains everything in between flat diamond layer and fully grown structures, and thus a gradient in structure height is clearly visible. In area 3, the fully grown structures are present, which are also fairly uniform throughout area 3. Raman spectroscopy has been performed on these molds to ensure the presence of diamond, results can be found in Appendix C.

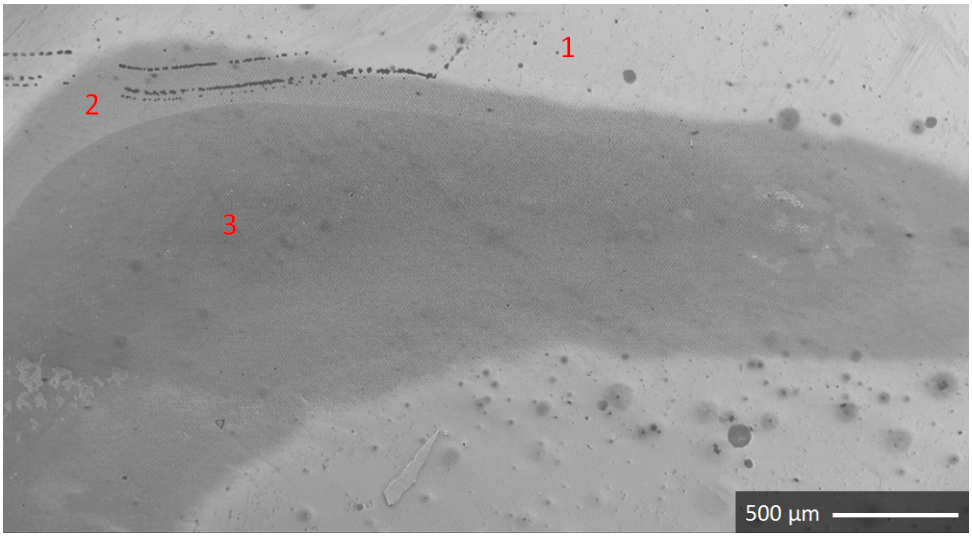

Figure 5.15: SEM image of a template-grown diamond mold, with the different areas indicated.

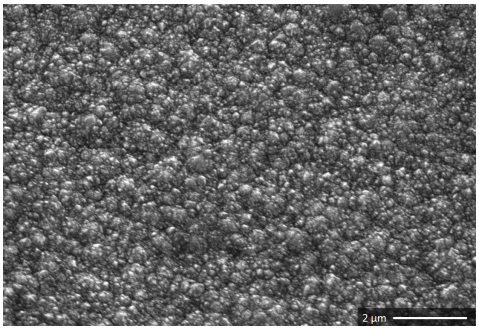

(a) Diamond structures in area 1.

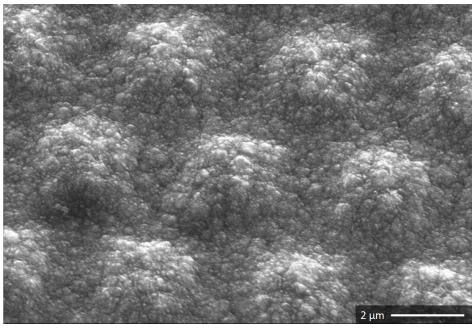

(b) Small diamond structures in area 2.

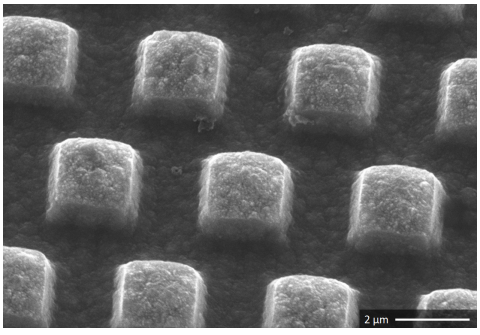

(c) Larger diamond structures in area 2.

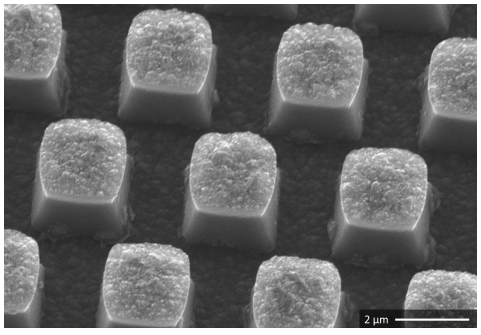

(d) Diamond structures in area 3.

Figure 5.16: 30° SEM images of variation of diamond structure height throughout template-grown sample.

5.5.2. IMPRINT INTO COC

In the foregoing imprint experiments, the optimal imprint temperature was determined to be around 170 °C. Therefore, all the imprint experiments with template grown diamond molds were done at this temperature. Likewise, the imprint duration was also be kept constant at 8 minutes, as was the case in previous experiments. The pressure of 10 MPa in previous imprint experiments was decreased to 3-4 MPa. Due to the larger size of the sample (about 2.5 x 2.5 cm) and the KOH etch, the wafer is more fragile. Imprinting with a lower pressure will therefore limit the risk of breaking the silicon substrate of the mold during the imprinting process. Because the sample is relatively large, graphite sheets were used during imprinting, as indicated in Appendix A.3.1.

After the mold production and imprint parameters have been determined (170 °C, 3-4 MPa, 8 minutes, 6 hours growth at standard conditions), the imprint experiments were performed. Imprinting experiments were done without any problem up until the releasing of the mold. Due to the size of the mold and the decreased thickness of the silicon substrate because of KOH etching, the mold was too fragile to be released without breaking. The four different molds tested in these experiments all came out of the imprinting setup intact but broke in the releasing process. Therefore, no replication of the experiment by using the same mold multiple times was possible. A solution for this problem might be using wafers with a thickness of 1 mm or more as basis for the stamp. It was possible, however, to release all the individual pieces from the broken mold and thereafter analyze the COC imprints.

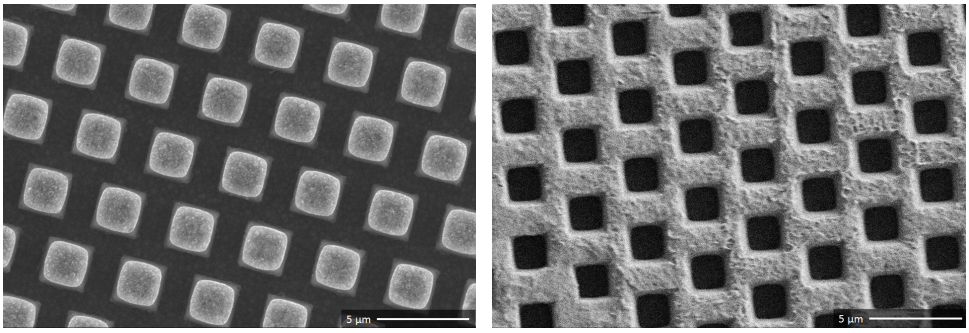

(a) Diamond mold. (b) Imprint into COC.

Figure 5.17: SEM images of the 6h template-grown mold together with the imprint into COC.

Analysis of the COC imprint was done by SEM, the top view images of this analysis are shown in Figure 5.17. Measurements of the dimensions at the bottom of the pyramid-like structure show that dimensions of both the diamond structures and the imprint are 2.5 x 2.5 μm. This also matches the dimensions of the porous template and indicates that the diamond neatly follows the pores during template growth.

Images of further analysis can be found in Figure 5.18. As can be seen, the diamond structures get a little wider towards the top of the structure. This an effect of the widening of the pores in the silicon template. Which could lead to the mold getting stuck in the COC, since the polymer could interlock with the mold. But, apparently, the release of

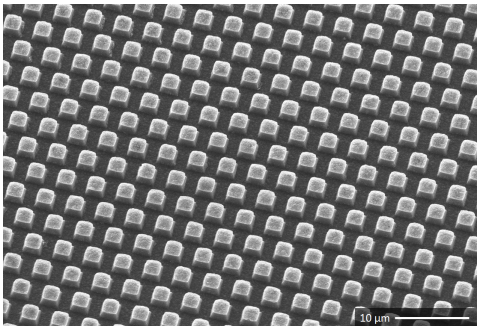

(a) FDTS-coated diamond structures.

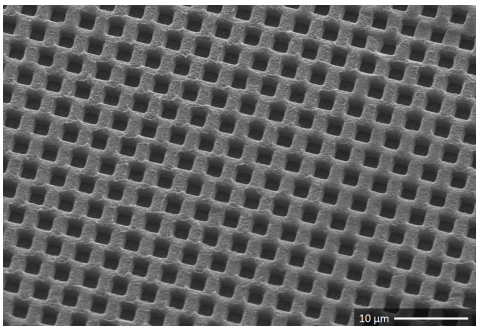

(b) COC imprint of template-grown stamp.

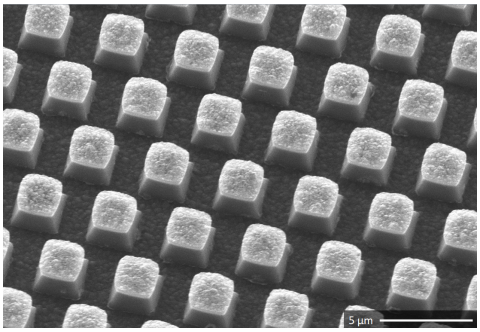

(c) FDTS-coated diamond structures.

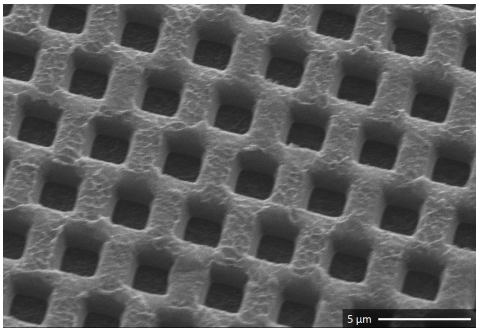

(d) COC imprint of template-grown stamp.

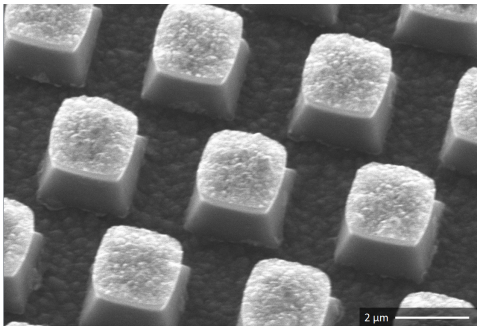

(e) FDTS-coated diamond structures.

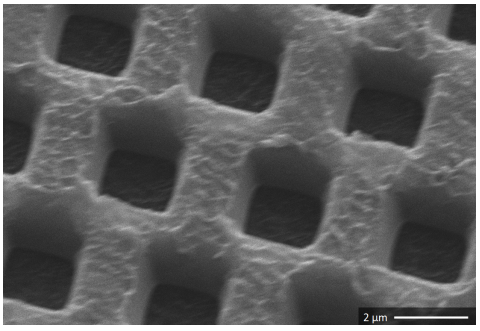

(f) COC imprint of template-grown stamp.

Figure 5.18: Comparison of mold (left column) and COC imprint (right column), images made under 30° with a SEM.

these structures was still possible. The structure of the COC imprint seems to match the structure of the diamond mold very well. Uniformity throughout the imprint was very good, some defects were visible, but on further inspection these defects occurred at spot were no diamond structures were grown.

CONCLUSIONS

In this thesis, a first step has been made to develop less complex and cheaper methods for the production of CVD diamond imprint stamps. Stamps were successfully produced by two different fabrication methods, i.e. the CVD coating of micro-structured silicon and the template synthesis of full diamond micro-structures. Both types of diamond stamps were then tested in thermal imprint lithography embossing of COC. A few conclusions can be drawn from this study:

- **Method 1 - CVD diamond coated micro-structured silicon**: synthesis of a 0.5 μm CVD diamond layer proved to be enough to cover silicon substrates with a closed diamond coating. However, the dimensions and the shape of the structures were altered as an effect of the diamond coating. On coated small structures protruding from the substrate an increase in lateral dimension from 0.7 μm to 1.5 μm, while dimensions of the circular depressions were decreased from 1.9 μm to 1.1 μm. This method is therefore not suited for structure dimensions of less than 1.5 μm. Imprinting of the stamps into COC without anti-adhesion layer proved that imprinting was also possible with the as-grown CVD diamond layer. Imprints of dimensions down to 1 μm with a depth of 350 nm have been realized.

- **Method 2 - Template-grown CVD diamond**: full diamond CVD imprint molds were fabricated by the synthesis of diamond through a micro-porous silicon template. With this method, diamond structures of 2.5 x 2.5 μm with a height of 2 μm on areas of up to 30 mm^2 were synthesized. Imprinting of theses samples into COC resulted in accurate replications of the molds.

- **Imprint parameters**: investigation of the imprint parameters showed that the best imprints into TOPAS®COC grade 6013 were realized 40 °C above the glass transition temperature. The optimal imprint pressure has been determined at 10 MPa for molds of about 1 x 1 cm^2 and 3-4 MPa for molds of 2 x 2 cm^2 - 3 x 3 cm^2. An imprint duration of 8 minutes proved to be sufficient in order to fully transfer the patterns into COC.

- **FDTS anti-adhesion layer**: although it was shown that imprinting with the standard CVD diamond layer (grown at CH_4 / H_2 ratio of 2%, 725°C, and 425 W filament power) is possible, the use of an anti-adhesion layer to make release of the mold easier is still advisable. FDTS proved to be suited for the purpose of anti-adhesion layer on a diamond coating. A significant increase in water contact angle from 80° to 95° and thereby a significant decrease in surface energy were shown after formation of a FDTS layer. Furthermore, it has been shown that coating by FDTS can be done by simply dispersing the mold in a solution of FDTS diluted in ethanol.

RECOMMENDATIONS FOR FUTURE RESEARCH

GENERAL RECOMMENDATIONS

- **Synthesizing UNCD or low roughness NCD diamond**: for imprint lithography, smooth surfaces of the mold structures are very important. There are still some possibilities to decrease the diamond layer roughness (roughness values of our diamond can be found in Appendix D.1). Two types of diamond layers could be further investigated, UNCD, and low roughness NCD diamond. UNCD seems to be the most promising of these two options, since its roughness is extremely low with a typical RMS roughness of 6 nm [45]. On the other hand, low roughness NCD contains more sp^2 carbon since it is grown at higher methane ratios and will therefore have a decreased hardness and wear resistance.

- **Durability tests**: one of the most prominent reasons of using diamond for imprint stamps is the likely decrease in the wear of the stamp, and thereby the increase in lifetime. Further research could be conducted in which the durability of both the CVD diamond coated micro-structured silicon and the template-grown molds are compared to standard untreated silicon molds (with the same structures). In addition, the life span of the FDTS anti-adhesion layer is also still unknown. Yet, similar layers have been investigated which resulted in a lifetime in the range of 1000's of imprint cycles [31]. However, life span of the anti-adhesion layer is less relevant than the durability of the stamp material, since it can be re-coated.

- **Imprinting into metals**: apart from being likely more durable, diamond can also be used to enable imprinting into materials that cannot be imprinted with standard mold materials. A start could be made by attempting to imprint into softer metals (highly pure aluminum and copper), which have a low hardness compared to other metals. If this proves successful, one can attempt to imprint into harder metals and even titanium. The template-grown molds seem to be best suited for imprinting into harder metals, since these molds contain full diamond structures.

- **Smaller structures and higher aspect ratios**: imprint molds fabricated and imprinted in this thesis had aspect ratios up to 1, and structure dimensions down to 1 μm. Further research could be done by investigating the fabrication and imprinting of structures with smaller dimensions and higher aspect ratios, ultimately enabling nanoimprint lithography of polymers and/or metals.

CVD DIAMOND COATED MICRO-STRUCTURED SILICON

- **Long trenches**: as discussed earlier, the checkerboard structures with a depth of 50 μm did not release. One of the possible reasons could be that air is not able to go inside the imprinted structures when trying to release the mold. Since the cubic structures are oriented as a checkerboard with closed corners, air cannot flow in during the release process and thus the imprint remains strongly attached to the mold due to vacuum. Therefore, the imprinting of long trenches stretching across the entire sample could be investigated. This would solve the problem of air not reaching the bottom of the imprinted structures.

- **Undercut**: all the silicon substrates used in this thesis consisted of structures perpendicular to the silicon wafer. While this exploits the benefits of imprint lithography, it is not contributing to an easy release of the mold. Therefore, structures with an undercut could be produced and tested for imprinting too. When an undercut is implemented, it is likely that structures with higher aspect ratios can be imprinted and released successfully.

- **Smooth structure walls**: as can be seen in Section 5.4.2, the deep silicon substrates contained rugged side walls. These rugged side walls increase the interlocking with the polymer when imprinting. Experiments could be done using silicon molds with smooth side walls in order to verify if deeper structures (50 μm) can be imprinted.

TEMPLATE GROWTH

- **Optimize template thickness**: as discussed earlier, growing through a template severely decreases diamond deposition rates (see Section 5.5). While this is an effect that is likely to be inevitable, the magnitude might be greatly decreased. Because the diamond deposition rate is expected to be greater near the top of the template, the template should ideally be as thick as the height of the desired features. Since this requires great control of the absolute diamond deposition rates, an initial investigation can be done using templates that are 2 μm thicker than the desired structure height (instead of the additional 16 μm used in this thesis).

- **Scaling up of template growth**: the porous silicon templates used in this thesis are 1 x 1 cm^2 in size. The scaling up of these porous templates to wafer size could be investigated. Succeeding in this task would enable the growth of structured diamond on wafer scale. When using larger wafers and porous templates, it is advisable to synthesize diamond with another sort of CVD tool, preferably a microwave CVD tool or a HFCVD setup with multiple filaments arranged in a parallel array.

- **Fixation of template to diamond layer**: due to the suboptimal fixation of the porous silicon template to the diamond layer underneath, the area of the structured diamond grown does not match the area of the porous template exposed to the CVD gas atmosphere. The largest structured area attained in this thesis was about one third of the template area (30 mm^2). Further research could be conducted to attempt to get a better connection between the flat diamond film and the porous

silicon template. A possible strategy could be relaxing of the template onto the diamond film by heat treatment.

- **Influence of porous template on diamond deposition rate**: a study could be conducted in which the effect of the porous silicon template on the diamond depositing rate is investigated. It is very likely that the effective deposition rate is a function of the template thickness and that it locally increases as the growing diamond pattern vertically approaches the top of the template, and thus that deposition rate is not constant. The effective diamond deposition rate throughout the porous silicon template is still not known.

- **Create different kinds of complex structures**: the template growth method allows the fabrication of complex diamond structures. Further research could be done regarding complex diamond structures that are suited for imprint lithography, as well as complex diamond structures that are not imprintable but have other applications. Possible applications could be: superhydrophobic surfaces, creation of full diamond membranes, and substrates for protein growth [37]. Basically, any shape can be made as long as there is still adequate exposure of the diamond growth front to the reactive CVD gases.

A

TECHNIQUES

A.1. SAMPLE ANALYSIS

A.1.1. SCANNING ELECTRON MICROSCOPY

Two SEMs have been used, for low resolution SEM images a Jeol JSM-6010LA Scanning Electron Microscope is used. High resolution SEM images have been made with a FEI Nova NanoSEM 450.

Since COC is not conductive, the polymer needs to be coated with a conductive layer in order to be able to make SEM images. All the COC imprints imaged with the SEM in this thesis are coated with 6.5 nm of gold/palladium (Au/Pd), on a Quorum Technologies SC7620.

The working principle of a SEM is quite similar to that of an optical microscope. But instead of light, electrons are used. A SEM consists of an electron gun which produces the electrons, these electrons are then accelerated by a high electric potential. A system of electromagnetic lenses focuses the electrons on the sample. When the incident electron beam hits the surface, backscattered and secondary electrons are emitted (among other things that will not be discussed). Backscattered electrons are electrons of the incident beam that hit a nucleus, these electrons lose relatively little energy in the process and thus have a high velocity. Secondary electrons are emitted when incident electrons collide with the electrons in the sample and knock them out of their usual orbit. Our SEM images are made using secondary electron imaging mode. By scanning across the surface, a raster image can be produced.

A.1.2. WHITE LIGHT INTERFEROMETRY

Heights are measured with a Bruker ContourGT-K1 white light interferometer. All height measurements have been done using white light, because this gives better resolution in that direction.

A white light interferometer is schematically shown in Figure A.1. Light emitted from the white light source (or other kinds of light) is partially reflected and partially transmitted by the half transparent mirror in the middle. This light then travels to the flat

reference mirror or the specimen, where it is reflected. After passing through the half transparent mirror again, an image can be formed on the CCD camera. This CCD camera records the interference signal as the specimen is scanned, the focus position of any point on the specimen's surface corresponds to the point of maximum fringe contrast. When the specimen is scanned vertically over the full height range, the position of maximum fringe contrast is found for each pixel and a 3D image can be formed.

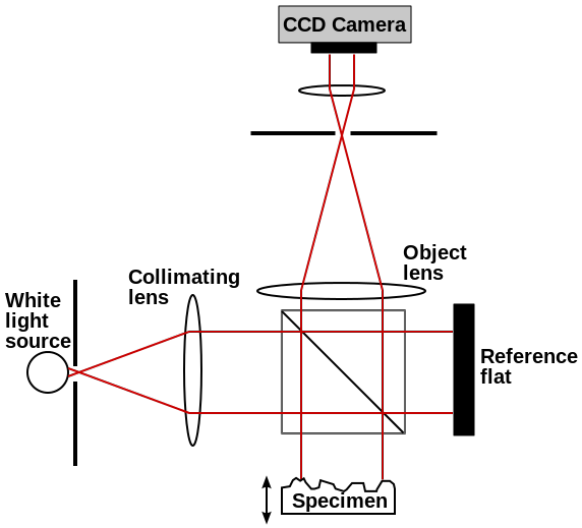

Figure A.1: Overview of a white light interferometer setup. Reproduced from [43].

A.1.3. RAMAN SPECTROSCOPY

The Raman spectroscope measurements were performed with a Horiba LabRAM HR setup, equipped with an argon ion laser operating at 514 nm. Spectrum acquisition was performed with 50x objective lens, 1800 lines/mm grating, 1000 μm hole aperture, integration time of 2 s accumulated 5 times, and no power attenuator. The spectral resolution under these conditions was ~0.3 cm^{-1}. The laser line (FWHM of 2.6 cm^{-1}) was used as reference for calibration.

Raman spectroscopy is a method to determine the molecules present in a sample. Raman spectroscopy relies on the inelastic scattering, or Raman scattering of monochromatic light. When the laser interacts with molecular vibrations, phonons or other excitations in the system, the energy of the laser phonons is being shifted up or down. This shift provides information about the molecular content of the sample analyzed.

A.2. SAMPLE MODIFICATION

OXYGEN PLASMA

Oxygen plasma is used in an attempt to oxidize the surface of the silicon substrates. Oxidation of the surface using oxygen plasma is done in a Diener Femto for 15 minutes at 99 W.

ACID TREATMENT

In order to make sure the surface is sufficiently oxidized or to remove sp2 carbon content, a mixture of concentrated acids was used. This mixture contains 70% concentrated nitric acid (HNO_3), 95% concentrated sulphuric acid (H_2SO_4), and 38% concentrated hydrochloric acid (HCl) in a 1:1:1 volume composition. After mixing the acids, the mixture together with the sample was boiled for about 10 minutes.

SEEDING

Seeding is done using a spincoater which is schematically represented in Figure A.2, for the sake of clarity the substrate and diamond solution belly have been enlarged. The substrate is placed in the middle of the stage and is held in place using vacuum. Then, a syringe is used to cover the whole substrate with the NanoAmando solution, ideally a clearly visible belly of fluid is present on the substrate. This belly is left on the substrate for at least 1 minute, thereafter the spincoater is turned on and is set at 2000 rpm for 1 minute. During the first 10 seconds, ethanol is dispersed onto the substrate in order to get rid of excess diamond particles, and to minimize agglomeration. When the substrate has stopped spinning, the seeding procedure is completed. It is very important that nothing touches the top surface of the sample after completion of the seeding procedure since the diamond seeds layer is extremely frail. Touching the surface, spraying it with gas or with a liquid will all remove diamond seeds from the surface, and thereby decrease the seeding density or remove all the seeds.

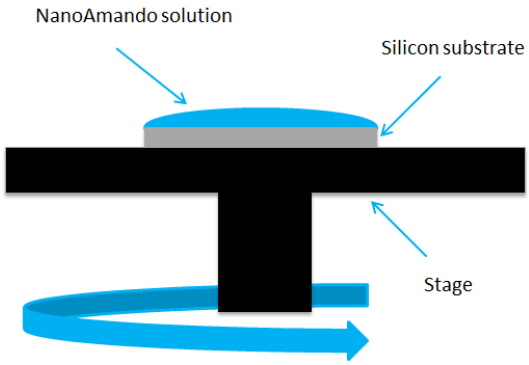

Figure A.2: Schematic representation of the spincoater.

A

HFCVD

Diamond growth is done in an in-house built HFCVD reactor, which can be seen in Figure A.3. The HFCVD machine consists of a CVD reactor, induction coil cooling, heating for the sample holder, power supply for the filament, and gas flow regulation. The filament used to activate the thermal induced plasma is made out of Tantalum. There are several steps involved in our standard growth protocol:

1. After placing the sample, the reactor is pumped down, the sample holder is preheated to 200°C, and the reactor is flushed with hydrogen gas a few times.
2. Methane and hydrogen gas flows are set to 6 sccm and 300 sccm respectively, resulting in a CH_4 / H_2 ratio of 2%.
3. The pressure is regulated to 10.0 mbar.
4. The sample holder temperature is increased to 725°C and the current through the filament is increased to 18.2 A, resulting in a filament power of about 425 W.
5. When the synthesis time has passed, the filament current and the sample holder temperature are set to 0, the methane flow is cut, and the reactor is left to cool down.

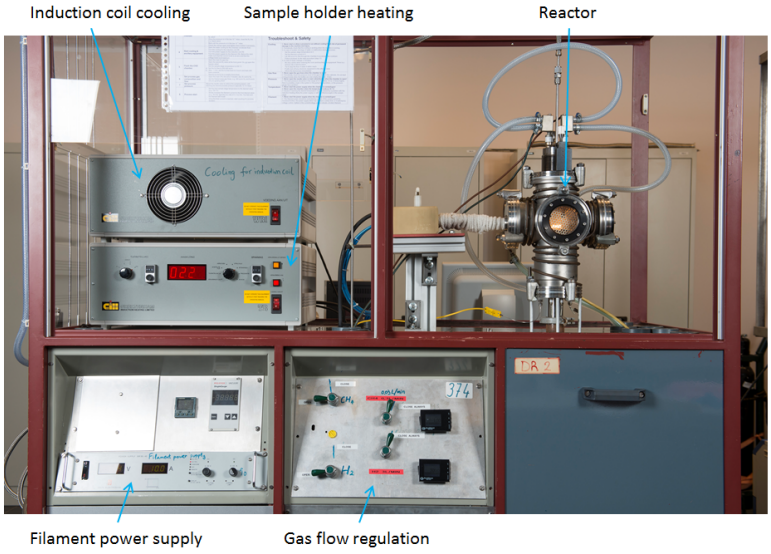

Figure A.3: Overview of the HFCVD reactor.

Further explanation of HFCVD can be found in Section 2.1.2.

A.3. IMPRINT LITHOGRAPHY

A.3.1. EXPERIMENTAL SETUP FOR THERMAL IMPRINT LITHOGRAPHY

For the imprint experiments in this thesis an EVG 510 wafer bonder is used, which is displayed in Figure A.4. This system allows to vary the imprint temperature, the imprint force, and the imprint time. The exact imprinting parameters can be found in Section 5.
The basic steps in the process are:

1. Heating of the polymer and mold.
2. Piston down, at imprint pressure.
3. Wait for set imprint time.
4. Cool down polymer and mold.
5. Piston up.

Figure A.4: EVG 510 wafer reproduced from [44].

The full recipe of the imprinting process can be found in Appendix A.3.2.

The layer buildup inside the EVG 510 system is done depending on the size of the molds. Small stamps of about 1 x 1 cm or smaller can be imprinted without graphite sheets, the kapton foil will compensate for small misalignments that may be present. However, for the bigger stamps, kapton foil alone is not enough to compensate for misalignment. Two graphite sheets, one big and one small are added to the layer buildup to prevent the stamp from breaking, an overview is shown in Figure A.5.

Figure A.5: Overview of the layer buildup for imprinting large samples.

A

A.3.2. THERMAL IMPRINT RECIPE

In Table A.1 the standard imprint recipe used for all the thermal imprint lithography experiments is reproduced. Within this recipe only 3 parameters are changed, these are: the imprint temperature (second Set Temperature), the imprint pressure (Piston Down), and the imprint time (Timer).

Table A.1: Standard imprint recipe for thermal imprint lithography experiments.

Command	Parameter 1	Parameter 2	Parameter 3	Parameter 4
Set Temperature	Heat Target: Both	Setpoint: 40 °C	Gradient: 20 °C/min	Allow active cooling: no
Wait Temperature	Heat Target: Both	Mode: higher	Temperature: 38 °C	
Evacuate	Mode: low			
Timer	Timer: 0:00:03.0 hh:mm:ss.s			
Wait Pressure	Mode: lower	Pressure: 1.000 mbar		
Flags	Left Flag: pull out	Center Flag: pull out	Right Flag: pull out	
Timer	Timer: 0:00:20.0 hh:mm:ss.s			
Evacuate	Mode: off			
Set Temperature	Heat Target: Both	Setpoint: 170 °C	Gradient: 20 °C/min	Allow active cooling: no
Wait Temperature	Heat Target: Both	Mode: higher	Temperature: 165 °C	
Piston Down	Setpoint: 1000 N	Gradient: max N/min		
Timer	Timer: 0:08:00.0 hh:mm:ss.s			
Purge	Mode: vent			
Wait Pressure	Mode: higher	Pressure: 800.0 mbar		
Purge	Mode: Off			
Set Temperature	Heat Target: Both	Setpoint: 30 °C	Gradient: 20 °C/min	Allow active cooling: no
Wait Temperature	Heat Target: Both	Mode: lower	Temperature: 55 °C	
Piston Up				

A.3.3. PDMS SOFT EMBOSSING PROTOCOL

Soft embossing into PDMS is done by mixing SLYGARD 184 silicone elastomer base with its curing agent in a 10:1 weight ratio, which is cast over the imprint mold in a petri dish. The petri dish is then put in a desiccator under low pressure in order to remove air bubbles in the PDMS. The petri dish containing the stamp and the PDMS is then baked in the oven for 1 hour at 70 °C in order to cure the PDMS. After which the PDMS can be removed from the mold.

B

MICRO-STRUCTURED SILICON SUBSTRATES

In this Appendix, the various silicon substrates used for fabrication of CVD diamond coated micro-structured silicon molds will be briefly discussed. Five different kinds of substrates are used, four of these substrates contain only square structures of a certain size. However, the multi-patterned substrate contains a wide range of different structure shapes with different sizes. An overview of all the samples is given in Table B.1, all exact structures present on the surface of the multi-patterned substrate can be found further in Table B.2 & B.3. Depth measurements are done using a white light interferometer and feature sizes are measured using a SEM (details about the tools can be found in Appendix A).

Table B.1: Feature sizes of all substrates.

Name	Trenches	Chessboard squares	Free standing squares	Circles	Depth	Die dimensions
Deep fully patterned	-	-	45x45 μm	-	47 μm	10x10 mm
Deep half patterned	-	50x50 μm	-	-	47 μm	10x10 mm
Shallow fully patterned	-	50x50 μm	-	-	500 nm	10x10 mm
Shallow half patterned	-	50x50 μm	-	-	500 nm	10x10 mm
Multi-patterned	1-100 μm	8x8 μm - 47x47 μm	5x5 μm - 49x49 μm	1.6 - 5 μm	350 nm	10x 5 mm

There are four dies that only contain one kind of feature. A distinction is made between the depth of the features and the layout of the substrate. Fully patterned substrates are uniform throughout, while half patterned substrates are half patterned and half flat as is shown in Figure B.1. Furthermore, deep substrates have a depth of 47 μm, while shallow substrates have a depth of 500 nm.

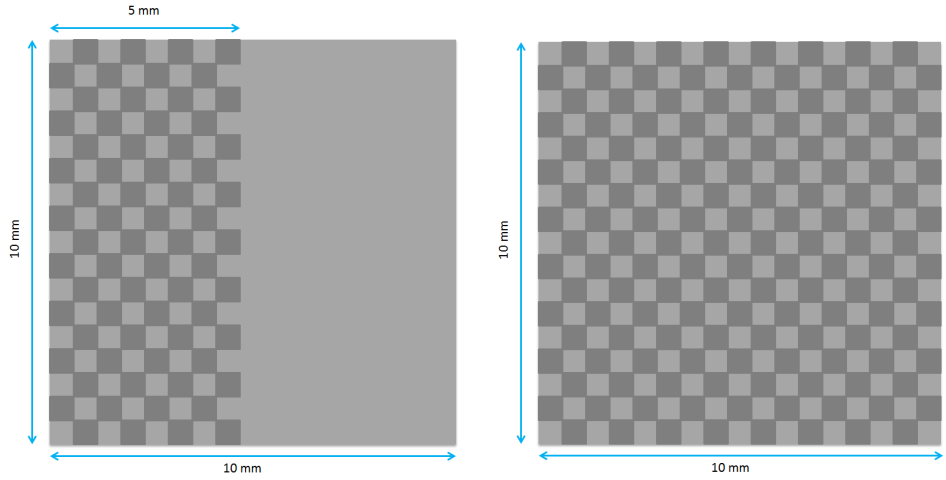

(a) Half patterned. (b) Fully patterned.

Figure B.1: Overview of the layout of the single-patterned substrates.

B.1. MULTI-PATTERNED SILICON SUBSTRATE

The multi-patterned contains different feature shapes (trenches, free standing squares, circles, and chessboard squares) in a wide variety of sizes. The edges of the squares become less distinct when the size gets smaller, therefore, the squares smaller than 5x5 μm are classified as circles. An overview image of the multi-patterned substrate is given in Figure B.2. However, the very small features are not visible in this image.

As is also clearly visible in the image, the substrate seems to be mirrored along the middle of the short side. This is however not the case, the bottom half as seen in the image contains structures coming out of the substrate and the top half contains structures etched into the substrate. All the structures present on the top half of the substrate can be found in Table B.2, and all the structures present on the bottom half of the substrate can be found in Table B.3.

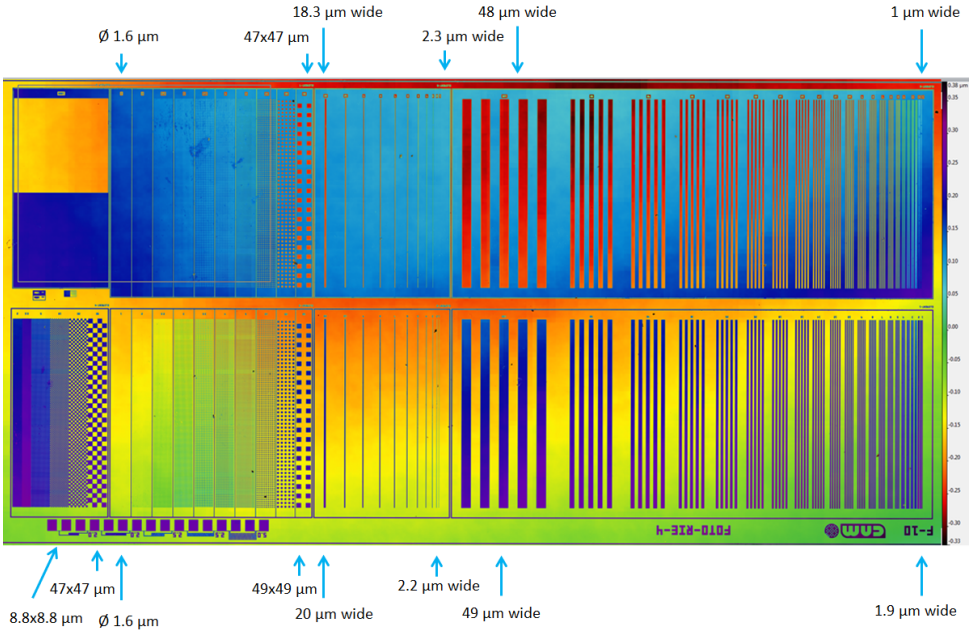

Figure B.2: Overview of the multi-patterned substrate, whitelighte interferometer image.

Table B.2: Protruding structure sizes on the top half of the substrate, 350 nm depth throughout.

Single trench	Multiple trenches	Circles (diameter)	Squares
2.3 μm	1 μm	1.6 μm	8.6x8.6 μm
2.8 μm	2.3 μm	2.5 μm	18x18 μm
4 μm	2.5 μm	3.2 μm	47x47 μm
4.9 μm	2.6 μm	4.3 μm	
5.8 μm	3 μm		
6.8 μm	4 μm		
7.6 μm	4.8 μm		
8.6 μm	5.8 μm		
18.3 μm	6.6 μm		
	7.7 μm		
	9 μm		
	11 μm		
	13 μm		
	14 μm		
	17 μm		
	18 μm		
	23 μm		
	28 μm		
	38 μm		
	48 μm		

Table B.3: Hole structure sizes on the bottom half of the substrate, depth is 350 nm throughout.

Single trench	Multiple trenches	Circles (diameter)	Squares	Chessboard squares
2.2 μm	1.9 μm	1.6 μm	10x10 μm	8.8x8.8 μm
2.9 μm	3 μm	3.2 μm	20x20 μm	18x18 μm
3.7 μm	3.5 μm	4.3 μm	49x49 μm	47x47 μm
4.7 μm	4 μm	4.8 μm		
5.6 μm	5 μm			
6.7 μm	6 μm			
7.6 μm	7 μm			
8.5 μm	8 μm			
9.6 μm	9 μm			
10.6 μm	10 μm			
20 μm	11 μm			
	13 μm			
	14.5 μm			
	17 μm			
	18 μm			
	20 μm			
	25 μm			
	30 μm			
	40 μm			
	49 μm			

B.2. SHALLOW FULLY PATTERNED SILICON SUBSTRATE

In Figure B.3, a 3D images made with a whitelight interferometer and top view SEM images of the shallow fully patterned substrate are displayed.

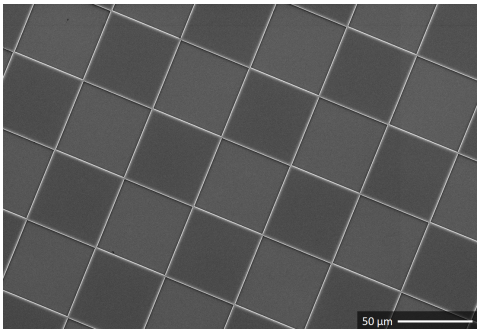

(a) Top view SEM image.

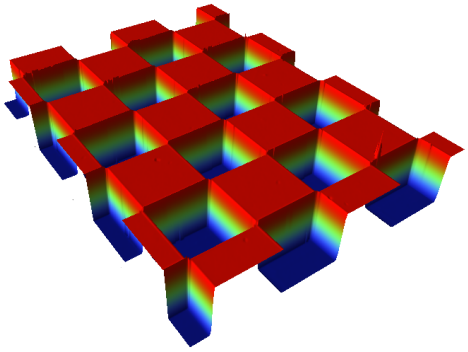

(b) 3D whitelight interferometer image.

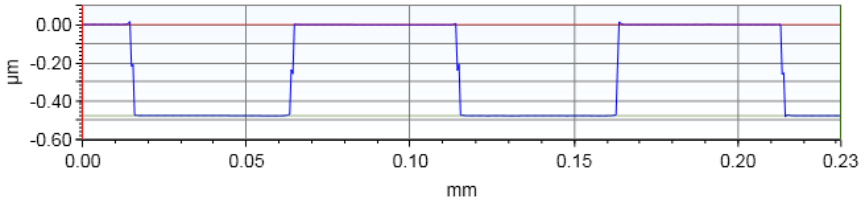

(c) Whitelight interferometer height profile.

Figure B.3: Images and data of shallow fully patterned silicon substrate.

B.3. SHALLOW HALF PATTERNED SILICON SUBSTRATE

In Figure B.4, a 3D images made with a whitelight interferometer and top view SEM images of the shallow half patterned substrate are displayed.

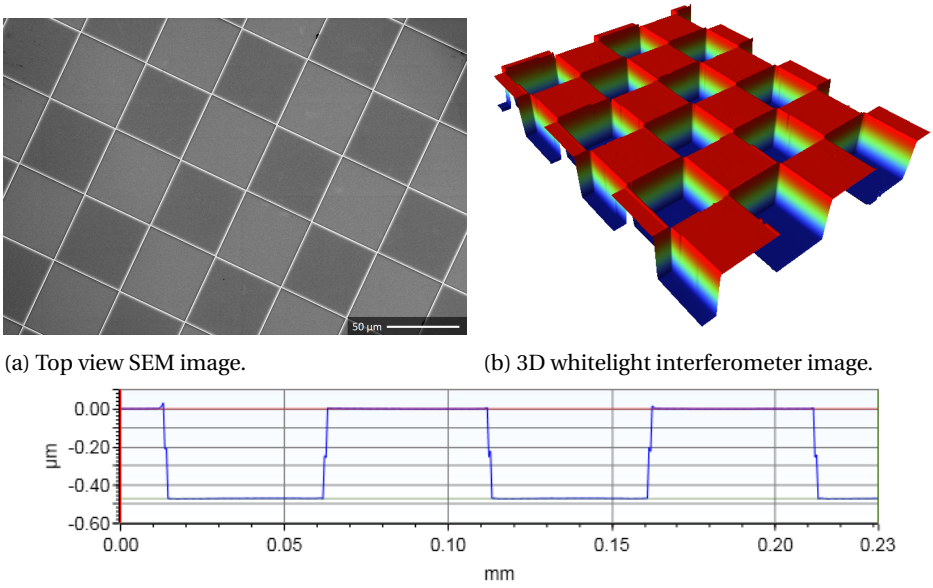

(a) Top view SEM image.

(b) 3D whitelight interferometer image.

(c) Whitelight interferometer height profile.

Figure B.4: Images and data of shallow half patterned silicon substrate.

B.4. DEEP FULLY PATTERNED SILICON SUBSTRATE

In Figure B.5, a 3D images made with a whitelight interferometer and top view SEM images of the deep fully patterned substrate are displayed.

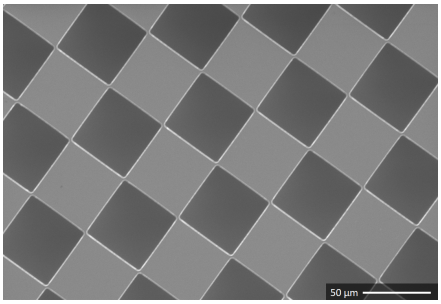

(a) Top view SEM image.

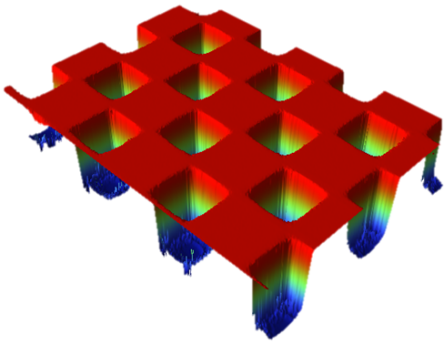

(b) 3D whitelight interferometer image.

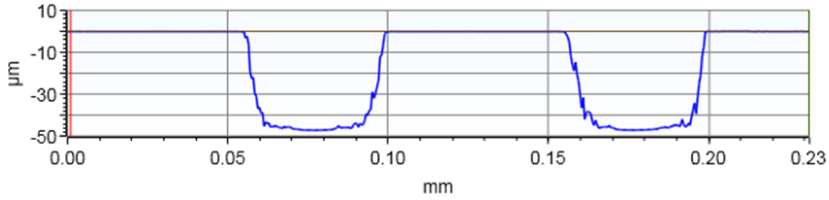

(c) Whitelight interferometer height profile.

Figure B.5: Images and data of deep fully patterned silicon substrate.

B.5. DEEP HALF PATTERNED SILICON SUBSTRATE

In Figure B.6, a 3D images made with a whitelight interferometer and top view SEM images of the deep half patterned substrate are displayed.

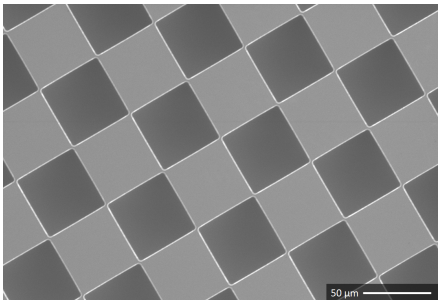

(a) Top view SEM image.

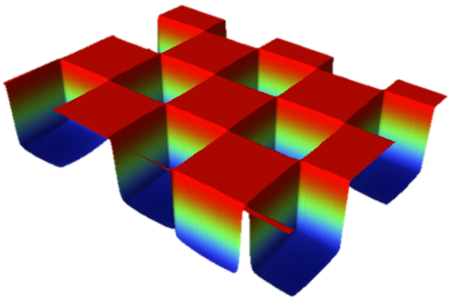

(b) 3D whitelight interferometer image.

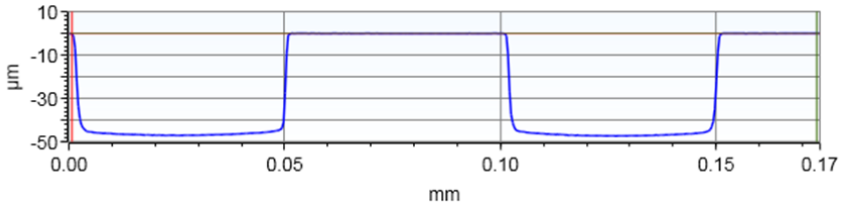

(c) Whitelight interferometer height profile.

Figure B.6: Images and data of deep half patterned silicon substrate.

C

RAMAN DATA

In this Appendix, the Raman data of the diamond layer resulting from the different mold production methods will be discussed. Raman analysis is done in order to confirm presence of diamond on the surface of our sample. The presence of diamond is indicated by an intensity peak at 1332 cm^{-1} [38]. Details of the Raman setup can be found in Appendix A.

The Raman plots of the diamond layers of both methods are displayed in Figure C.1 and Figure C.2. Raman data of both samples is plotted from 1000 cm^{-1} upwards, because the diamond peaks are otherwise poorly visible due to the existence of a very large silicon peak. The diamond peaks at 1332 cm^{-1} are clearly visible in both plots. Also the peak at 1472 cm^{-1} is found, this is peak is attributed to sp^2 material at the grain boundaries. This peak therefore gives an indication of the number of grain boundaries, and thereby the type of diamond, NCD in this case. A peak at 1560 cm^{-1} is the so called G peak, and also indicates the presence of non-diamond sp^2 material. The peaks at 1130 cm^{-1} can be attributed to non-crystalline transpolyacetylene in grain boundaries of nanocrystalline diamond, the presence of these peaks also confirms that NCD is synthesized [39].

STANDARD 0.5 μM DIAMOND LAYER

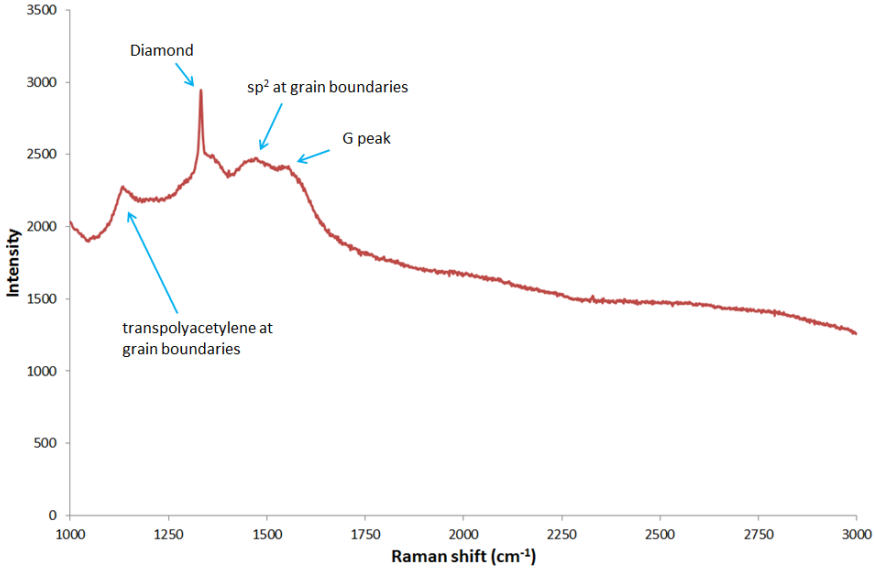

Figure C.1: Raman plot of a standard 0.5 μm diamond layer.

TEMPLATE GROWN DIAMOND LAYER

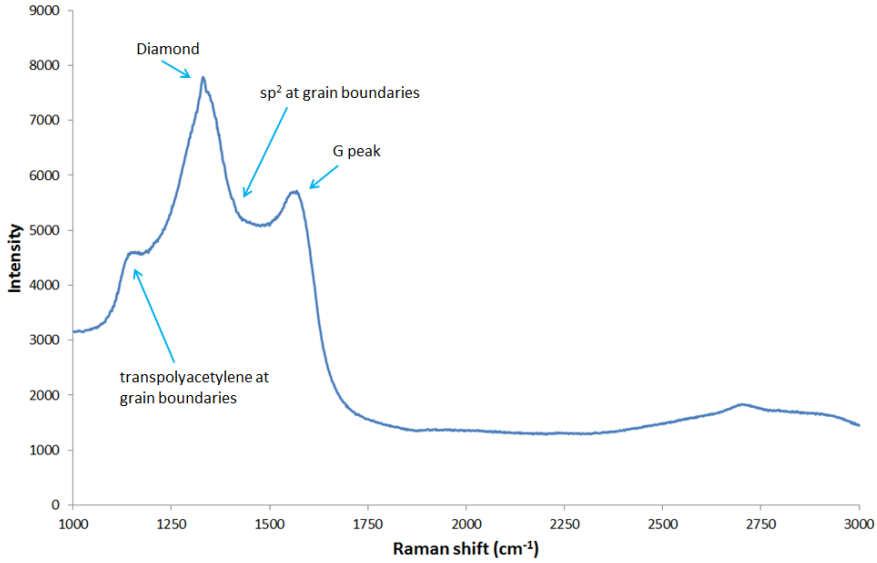

Figure C.2: Raman plot of a template grown diamond layer.

D

SURFACE PARAMETERS

D.1. ROUGHNESS

Since roughness is a major component in the quality of an imprint mold, the roughnesses of a 0.5 μm standard CVD diamond layer has been measured. But first, the theory behind these surface roughness measurements will be discussed briefly. There are different parameters to characterize the roughness profile of the sample, depending on the application different parameters are used.

- S_a gives the arithmetical mean of the absolute values of the profile deviations from the mean line of the roughness profile.
- S_q represents the root mean square value of height variations within the defined area.
- S_y indicates the difference in height between the deepest pit and the highest peak and can therefore be calculated by adding S_p to the absolute value of S_v.
- S_p gives the value of the height of the highest peak within the area measured from the mean value.
- S_v indicates the value of the depth of the deepest pit within the area measured from the mean value.

Surface roughness measurements are done using a Nanosurf Nanite AFM system in combination with a contact cantilever. The measurements are performed on a flat piece of 0.5 μm diamond grown under standard conditions (CH_4/ H_2 ratio of 2%, 725°C, and 425 W filament power).

Table D.1: Roughness values diamond sample.

Area	25x25 μm
Sa	8.6444 nm
Sq	10.973 nm
Sy	96.646 nm
Sp	59.701 nm
Sv	-36.945 nm

The RMS roughness of the nanocrystalline CVD diamond layer is approximately 11 nm, which is fairly low compared to literature. Usually RMS roughness of a CVD diamond layer is in the range of 15 to 40 nm [46]. The low roughness of our CVD diamond layer could be an effect of the relatively thin film and the use of 2% methane.

D.2. SURFACE ENERGY

By measuring the surface energy, an indication of the quality of deposition of the anti-adhesion layer as well as the effect of the anti-adhesion layer on the adhesion of the mold can be determined. Surface energy can be calculated from contact angle experiments using Young's equation:

$$\Upsilon_{SG} = \Upsilon_{SL} + \Upsilon_{LG}\cos\theta$$

- Υ_{SG} gives the surface energy of the solid material.
- Υ_{SL} is the interfacial tension between the solid and liquid.
- Υ_{LG} represents the surface tension of the liquid.
- $\cos\theta$ is the contact angle between the solid and the liquid.

Υ_{LG} is a property of the fluid used for contact angle experiments, and θ is experimentally determined. In this thesis contact angle measurements are done with an OneAttension Theta Optical Tensiometer. Contact angle measurements are done by dropping 3 μL of a specific fluids on the substrate, after which the contact angle can be measured. These measurements are always done on a flat unstructured sample, therefore the standard 0.5 μm CVD diamond layer has been synthesized on a flat silicon substrate. An example of a contact angle measurement is shown in Figure D.1, in this specific measurement DI water was dropped onto a FDTS dispersion-coated flat CVD diamond layer.

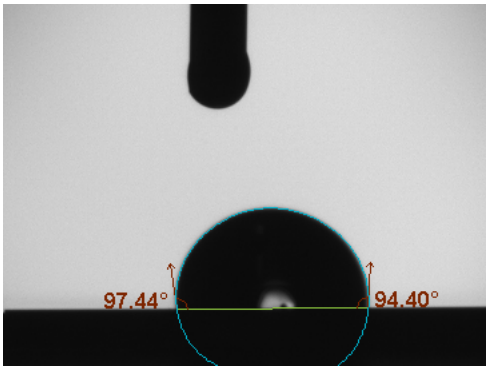

Figure D.1: Contact angle measurement of a 3 μL drop of DI water on FDTS dispersion-coated CVD diamond.

However, in order to solve the equation, Υ_{SL} has to be estimated. This can be done using several methods. For the sake of completeness, results of all the methods are displayed in Table D.2. More information about these methods can be found in papers by Volpe et al., Siboni et al., Kwok et al. [40–42]. In order to be able to apply these methods, different fluids have to be used. The fluids used are water (H_2O), ethylene glycol ($C_2H_6O_2$), and diiodomethane (CH_2I_2). All fluids are dropped in volumes of 3 μL, after which the contact angle is measured 17 times per second for 10 seconds. These measurements are then averaged to come to a final contact angle value.

Table D.2: Surface energy values.

Method	Without anti-adhesion γ_{tot} [mN/m]	Coated with FDTS γ_{tot} [mN/m]
Acid-Base	45	30
Equation of State	39	34
OWRK/Fowkes	49	40
Wu	52	42

The results in the Table above correspond reasonable well to the results found by Ostrovskaya et al., their measurements on hydrogenated diamond films resulted in a surface energy of 47 mN/m [47].

E

ADDITIONAL SEEDING IMAGES

In Figure E.1, an image of one of the smallest features seeded is shown. As can be seen, even in a trench that is no more than 100 nm wide at certain spots, dense seeding can be achieved through our seeding procedure (which can be found in Appendix A.2). When taking a closer look, one can see that there are even diamond seeds in the small holes in the sample.

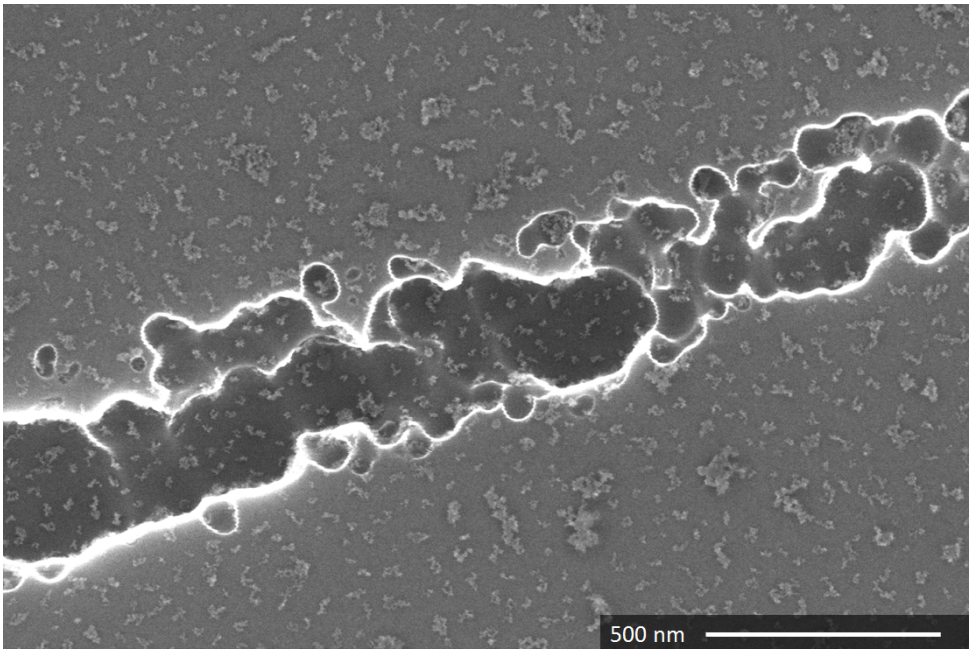

Figure E.1: SEM image of a small trench with dense seeding.

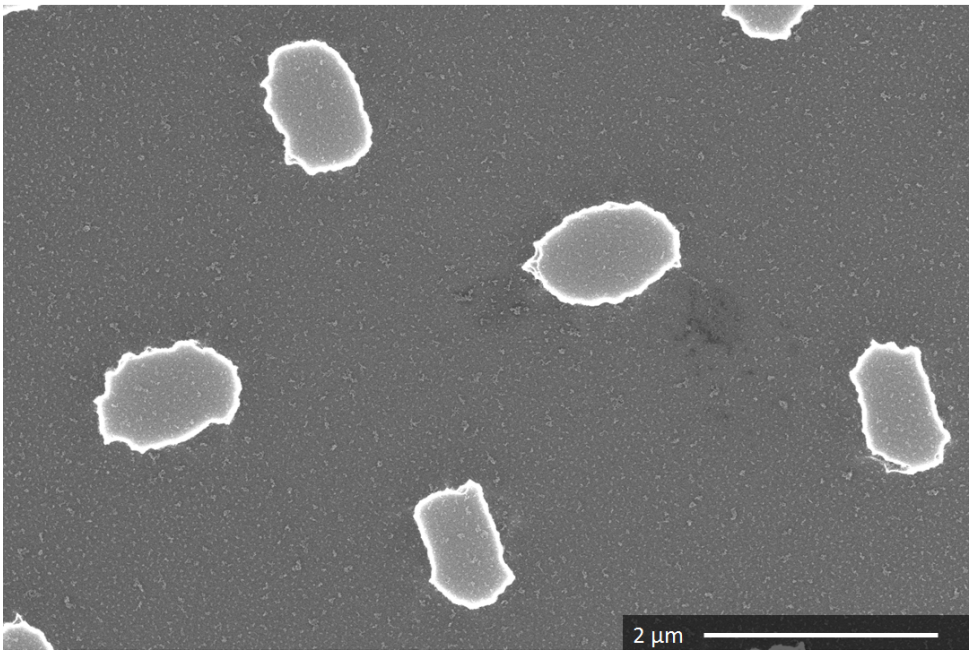

Figure E.2: SEM image of the diamond nanoparticle layer on small structures.

F

TEMPLATE GROWTH

During template growth of the CVD diamond imprint molds, structures were fabricated that cannot be transfered using imprint lithography. This Appendix will briefly discuss these structures, because while they are not suited for the purpose of this thesis, the structures are very interesting and cannot be produced with standard mass production methods. As mentioned in Section 4.2, the diamond grown through the template will follow the shape of the pores in the template. This enables the growth of very complex structures that can get thinner and wider throughout the height of the structure. In Figure F.1 a side view image of the porous silicon template and a schematic representation of the structures grown for 9 hours under standard conditions are shown.

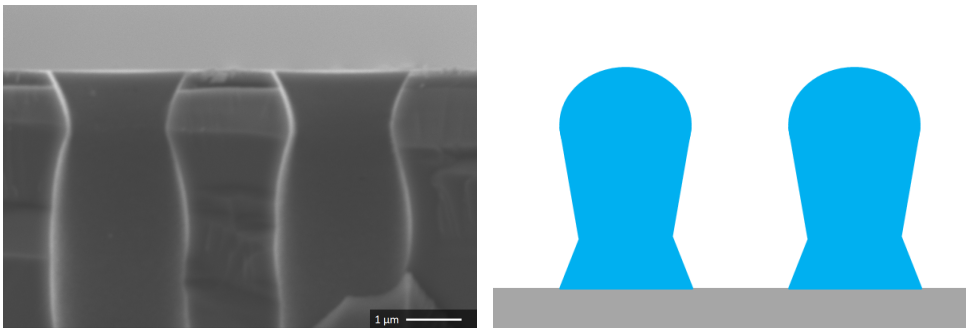

(a) SEM side view of the porous silicon template. (b) Resulting diamond structure after 9h growth.

Figure F.1: 9h diamond structure growth.

The Figures above clearly show that the height of structures suited for imprint lithography is limited to about 1.5 μm. Beyond this height the structure gets wider again, which results in the mold interlocking with the polymer while imprinting. But, this problem is specific to this porous template, if higher structures suited for imprinting were desired the template could be designed differently to facilitate the higher structures.

Since the area grown using the pattern grown method is limited by the area of the template or the area of the CVD plasma, this method is suited for synthesizing large areas (wafer scale) of structured diamond, as long as equipment permits. In Figure F.2, an SEM image of diamond structures after 9h of template growth is shown. As is visible in the image uniformity of the structures seems to be very good, both in the shape of the structures and the patterning throughout the sample.

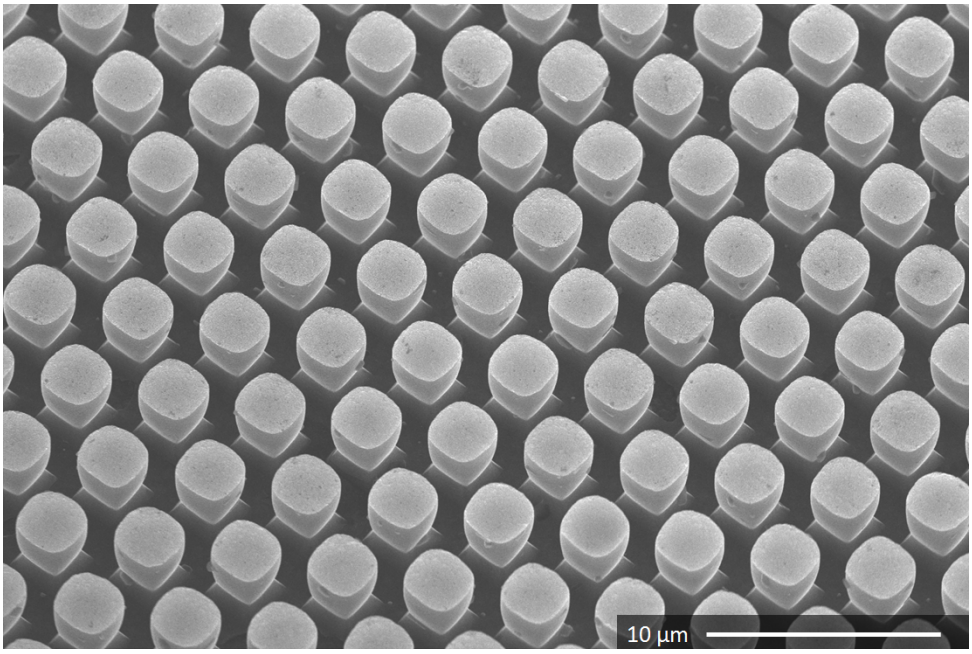

Figure F.2: Overview 30° SEM image of diamond structures grown 9h through a porous silicon template.

An overview image of the 9h template-grown diamond mold is shown in Figure F.3. This image has been taken using a Keyence optical microscope. In this image, the structured area is clearly visible due to the rainbow effect coming from the gradient in structure height. The square shape shows the location were the template was during diamond synthesis, and the rectangular shapes on the corners show the position of the pieces of silicon used to mechanically fixate the template.

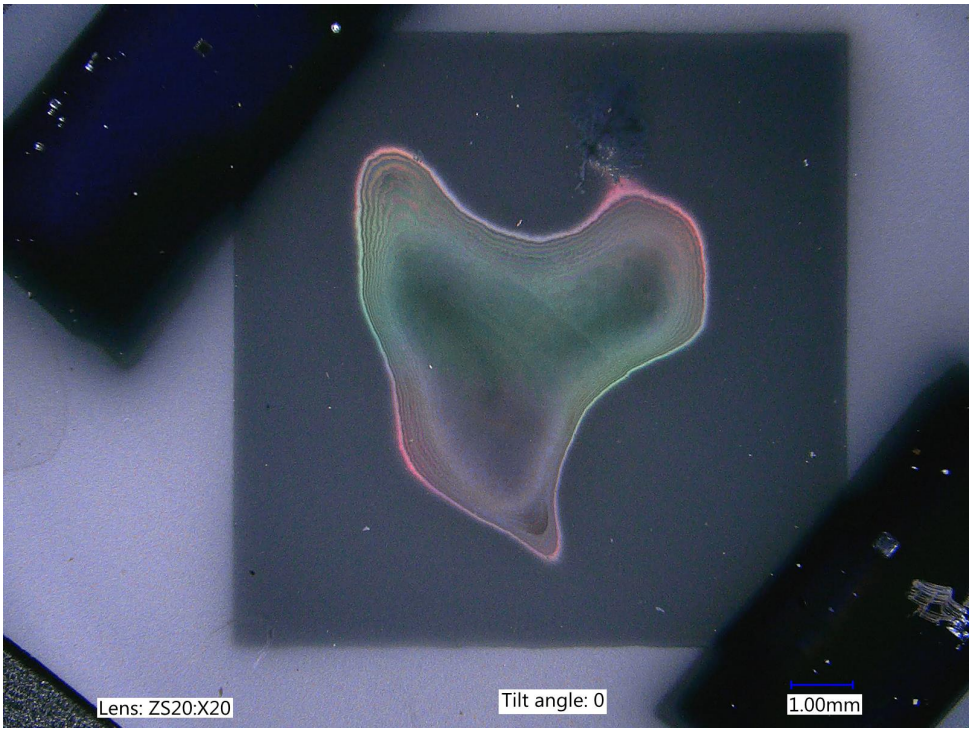

Figure F.3: Optical microscope overview image of the 9h template-grown diamond mold.

G

TOPAS®COC PROPERTIES

The properties of TOPAS®COC as obtained from the 2014 TOPAS Brochure E can be found in Table G.1.

Table G.1: TOPAS®COC properties.

Property	Unit	Test method	8007	6013	6015	5013	6017
Volume flow index MVR at 260 °C, 2.16 kg	ml/10 min	ISO 1133	32	14	4	48	1.5
Volume flow index MVR at HDT +115 °C, 2.16 kg	ml/10 min	ISO 1133	2	6	5	24	5
Density	g/cm³	ISO 1183	1.02	1.02	1.02	1.02	1.02
Water absorption (24 h immersion in water at 23 °C)	%	ISO 62	< 0.01	< 0.01	< 0.01	< 0.01	< 0.01
Water vapour permeability (at 23 °C and 85% relative humidity)	g · mm/ m² · d	DIN 53 122	0.023	0.035	0.035	0.030	0.045
Mold shrinkage (ϑ_W = 60 °C, 2 mm wall thickness)	%	–	0.1 - 0.5	0.4 - 0.7	0.4 - 0.7	0.4 - 0.7	0.4 - 0.7
Mechanical properties, measured under standard conditions, ISO 291 – 23/50							
Tensile strength [5 mm/min]	MPa	ISO 527 parts 1 and 2	63	63	60	46	58
Elongation at break [5 mm/min]	%	ISO 527, parts 1 and 2	10*)	2.7	2.5	1.7	2.4
Tensile modulus [1 mm/min]	MPa	ISO 527, parts 1 and 2	2600	2900	3000	3200	3000
Impact strength (Charpy)	kJ/m²	ISO 179/1eU	20	15	15	13	15
Notched impact strength (Charpy)	kJ/m²	ISO 179/1eA	2.6	1.8	1.6	1.6	1.6
Ball indentation hardness, 30-sec value	N/mm²	ISO 2039 part 1, applied load 961N	130	184	184	184	191
Thermal properties							
Heat deflection temperature HDT/B (0.45 MPa)	°C	ISO 75 parts 1 and 2	75	130	150	130	170
Coefficient of linear thermal expansion	K^{-1}	ISO 11 359 parts 1 and 2	$0.7 \cdot 10^{-4}$	$0.6 \cdot 10^{-4}$	$0.6 \cdot 10^{-4}$	$0.6 \cdot 10^{-4}$	$0.6 \cdot 10^{-4}$
Electrical properties							
Relative permittivity ε_r at 1-10 kHz	–	IEC 60250	2.35	2.35	2.35	2.35	2.35
Comparative tracking index CTI	–	IEC 60112	> 600	> 600	> 600	> 600	> 600
Volume resistivity	Ω · m	IEC 60093	$> 10^{14}$	$> 10^{14}$	$> 10^{14}$	$> 10^{14}$	$> 10^{14}$
Flammability							
UL Flammability Rating	Class	UL 94	HB (1.6mm)	HB (1.6mm)	HB (1.6mm)	HB (1.6mm)	HB (1.6mm)
Optical properties							
Light transmission (2 mm wall thickness)	%	ISO 13468-2	91	91	91	91	91
Refractive index	–	–	–	–	–	1.53	–
Abbe number	–	–		–	–	56	–

*) Yield strain: 4.5%

REFERENCES

[1] S.Veprek, "The search for novel, superhard materials", *Journal of Vacuum Science & Technology A: Vacuum, Surfaces, and Films*, Vol. 17, p.2401, 1999.

[2] H. O. Pierson, Handbook of Carbon, Graphite, Diamond and Fullerenes, Park Ridge, New Jersey (U.S.A.): Noyes Publications, 1993.

[3] C.Staats, 2016, https://tex.stackexchange.com/questions/141363/draw-realistic-3d-crystal-structures-diamond, accessed at 15 Nov. 2017.

[4] A.R. Lang, "Glimpses into the growth history of natural diamonds", *Journal of crystal growth*, Vol. 24-25, p. 108-115, 1974.

[5] O. A. Williams, M. Daenen, J. D'Haen, K. Haenen, J. Maes, V. V. Moshchalkov, M. Nesladek and D. M. Gruen, "Comparison of the growth and properties of ultrananocrystalline diamond and nanocrystalline diamond," *Diamond and Related Materials*, Vol. 15, p. 654, 2006.

[6] P. W. May, M. N. R. Ashfold and Y. A. Mankelevich, "Microcrystalline, nanocrystalline, and ultrananocrystalline diamond chemical vapor deposition: Experiment and modeling of the factors controlling growth rate, nucleation, and crystal size," *Journal of Applied Physics*, Vol. 101, p. 053115, 2007.

[7] Josephus G. Buijnsters, Luis Vazquez, "Growth Dynamics of Nanocrystalline Diamond Thin Films Deposited by Hot Filament Chemical Vapor Deposition: Influence of Low Sticking and Renucleation Processes", *The Journal of Physical Chemistry C*, Vol. 115, p. 9681-9691.

[8] M. Tsigkourakos, "Nucleation and Growth of Boron-doped Diamond Films for Electrode Application", April 2014.

[9] R. Gat, J.C. Angus, "Properties and Growth of Diamond", p. 325, 1994.

[10] M. Schwander, K. Partes, "A review of diamond synthesis by CVD processes", *Diamond and Related Materials*, Volume 20, Issue 9, p. 1287-1301, 2011.

[11] A.R. Kraussa, O. Auciellоa, D.M. Gruena, A. Jayatissa, A. Sumant, J. Tucek, D.C. Mancini, N. Moldovan, A. Erdemir, D. Ersoy, M.N. Gardos, H.G. Busmann, E.M. Meyer, M.Q. Ding, "Ultrananocrystalline diamond thin films for MEMS and moving mechanical assembly devices", *Diamond and Related Materials*, Vol. 10, 2001.

[12] V. L. Kuznetsov, M. N. Aleksandrov, I. V. Zagoruiko, A. L. Chuvilin, E. M. Moroz, V. N. Kolomiichuk, V. A. Likholobov, P. M. Brylyakov and G. V. Sakovitch, "Study of ultradispersed diamond powders obtained using explosion energy," *Carbon*, Vol. 29, p. 665, 1991.

[13] A. Krueger, "The structure and reactivity of nanoscale diamond," *Journal of Materials Chemistry*, Vol. 18, p. 1485, 2008.

[14] Stephen Y. Chou, Peter R. Krauss, Preston J. Renstrom, "Imprint of sub-25 nm vias and trenches in polymers", *Applied Physics Letters*, Vol. 67, No. 21, p. 3114, 1995.

[15] Stephen Y. Chou, Peter R. Krauss, Preston J. Renstrom, "Nanoimprint lithography", *Journal of Vacuum Science & Technology B*, Vol. 14, p. 4129, 1996.

[16] Stephen Y. Chou, Peter R. Krauss, Preston J. Renstrom, "Imprint lithography with 25-Nanometer Resolution", *Sience*, Vol. 272, Issue 5258, p.85-87, 1996.

[17] H. Schift, "Nanoimprint lithography: An old story in modern times? A review", *Journal of Vacuum Science & Technology B*, Vol. 26, p. 458, 2008.

[18] Stefan Landis, Tanguy Leveder, Nicolas Chaix, Cecile Gourgon, "Investigation of capillary bridges growth in NIL process", *23rd European Mask and Lithography Conference*, 2007.

[19] D.T. Tran, T.A. Grotjohn, D.K. Reinhard, J. Asmussen, "Microwave plasma-assisted etching of diamond", *Diamond & Related Materials*, Vol. 17, p. 717-721, 2008.

[20] D.T. Tran, C. Fansler, T.A. Grotjohn, D.K. Reinhard, J. Asmussen, "Investigation of mask selectivities and diamond etching using microwave plasma-assisted etching", *Diamond & Related Materials*, Vol. 19, p. 778-782, 2010.

[21] Jun Taniguchi, Yuji Tokano, Iwao Miyamoto, Masanori Komuro, Hiroshi Hiroshima, Kazuhiko Kobayashi, Takeshi Miyazaki and Hideyuki Ohyi, "Preparation of Diamond Mold Using Electron Beam Lithography for Application to Nanoimprint Lithography", *Japanese Journal of Applied Physics*, Vol. 39, p. 7070, 2000.

[22] Jun Taniguchi, Yuji Tokano, IwaoMiyamoto, Masanori Komuro and Hiroshi Hiroshima, "Diamond nanoimprint lithography", *Nanotechnology*, Vol. 13, p. 592, 2002.

[23] Yoshihiko Hirai, Satoshi Yoshida, Nobuyuki Takagi, Yoshio Tanaka, Hideki Yabe, Kei Sasaki, Hiroaki Sumitani and Kazuhiro Yamamoto, "High Aspect Pattern Fabrication by Nano Imprint Lithography Using Fine Diamond Mold", *Japanese Journal of Applied Physics*, Vol. 42, p. 3863, 2003.

[24] M Komori, H Uchiyama, H Takebe, T Kusuura, K Kobayashi, H Kuwahara and T Tsuchiya, "Micro/nanoimprinting of glass under high temperature using a CVD diamond mold", *Journal of Micromechanics and Microengineering*, Vol. 18, p. 065013, 2008.

[25] A. I. M. Greer, K. Seunarine, A. Z. Khokhar, X. Li, D. A. J. Moran, and N. Gadegaard, "Direct nanopatterning of commercially pure titanium with ultra-nanocrystalline diamond stamps", *Physica Status Solodi A*, No. 9, p. 1721, 2012.

[26] Bharat Bhushan and Xiaodong Li, "Micromechanical and tribological characterization of doped single-crystal silicon and polysilicon films for microelectromechanical systems devices", *Journal of Materials Sience*, Vol. 12, No. 1, 1997.

[27] Helmut Schift, Sina Saxer, Sunggook Park, Celestino Padeste, Uwe Pieles, and Jens Gobrecht, "Controlled co-evaporation of silanes for nanoimprint stamps", *Nanotechnology*, Vol. 16, p. S171-S175, 2005.

[28] Jin-Hwan Lee, Erik T. K. Peterson, Gabriel Dagani, Ian Papautsky, "Rapid prototyping of plastic microfluidic devices in cyclic olefin copolymer (COC)", *Proceedsing of SPIE*, Vol. 5718, 2005.

[29] O. Shenderova, S. Hens and G. McGuire, "Seeding slurries based on detonation nanodiamond in DMSO", *Diamond and Related Materials*, Vol. 19, p. 260, 2010.

[30] L. Ostrovskaya, V. Perevertailo, V. Ralchenko, A. Saveliev, V. Zhuravlev, "Wettability of nanocrystalline diamond films", *Diamond and Related Materials*, Vol. 16, p. 2109-2113, 2007.

[31] Nick R. Glass, Ricky Tjeung, Peggy Chan, Leslie Y. Yeo, and James R. Friend, "Organosilane deposition for microfluidic applications", *Biomicrofluidics*, Vol. 5, 2011.

[32] Pedro S. Nunes, Pelle D. Ohlsson, Olga Ordeig, Jorg P. Kutter, "Cyclic olefin polymers: emerging materials for lab-on-a-chip applications", *Microfluid Nanofluid*, Vol. 9, 2010.

[33] Valentina Doushkina, Erik Fleming, "Optical and mechanical design advantages using polymer optics", *Proceedings of SPIE*, Vol. 7424, 2009.

[34] Menelaos Tsigkourakos, Thomas Hantschel, Stoffel D. Janssens, Ken Haenen, and Wilfried Vandervorst, "Spin-seeding approach for diamond growth on large area silicon-wafer substrates", *Physica Status Solodi A*, No. 9, p. 1659-1663, 2012.

[35] Bongsoo Kim, Minwoo Park, Youn Sang Kim, and Unyong Jeong, "Thermal Expansion and Contraction of an Elastomer Stamp Causes Position-Dependent Polymer Patterns in Capillary Force Lithography", *Applied Materials & Interfaces*, Vol.3, p. 4695-4702, 2011.

[36] Kazuo Sato, Mitsuhiro Shikida, Yoshihiro Matsushima, Takashi Yamashiro, Kazuo Asaumi, Yasuroh Iriye, Masaharu Yamamoto, "Characterization of orientation-dependent etching properties of single-crystal silicon: effects of KOH concentration", *Sensors and Actuators A: Physical*, Vol. 64, Issue 1, p. 87-93, 1998.

[37] U. Meyer, A. Büchter, H.P. Wiesmann, U. Joos and D.B. Jones, "Basic Reactions of Osteoblasts on Structured Material Surfaces", *European Cells and Materials*, Vol. 9, p.39-49, 2005.

[38] Steven Prawer, Robert J. Nemanich, "Raman spectroscopy of diamond and doped diamond", *Philosophical Transactions of the Royal Society A*, Vol. 362, p. 2537, 2004.

[39] O. Ternyak, A.A. Cimmino, S. Prawer, A. Hoffman, "Ultrathin continuous undoped diamond films: Investigation of nanoscale conduction properties", *Diamond and Related Materials*, Vol. 14, p. 272-278, 2005.

[40] C. Della Volpe, D. Maniglio, M. Brugnara, S. Siboni, and M. Morra, "The solid surface free energy calculation I. In defense of the multicomponent approach", *Journal of Colloid and Interface Sience*, Vol. 271, Issue 2, p. 434-453, 2004.

[41] S. Siboni, C. Della Volpe, D. Maniglio, and M. Brugnara, "The solid surface free energy calculation II. The limits of the Zisman and of the “equation-of-state” approaches", *Journal of Colloid and Interface Sience*, Vol. 271, Issue 2, p. 454-472, 2004.

[42] D.Y. Kwok, A.W. Neumann, "Contact angle measurement and contact angle interpretation", *Advances in Colloid and Interface Sience*, Vol. 81, Issue 3, p.167-249, 1999.

[43] https://en.wikipedia.org/wiki/White_light_scanner, accessed at 12 Feb. 2018.

[44] https://www.evgroup.com/en/products/bonding/waferbonding/evg510semi/, accessed at 18 Dec. 2017.

[45] Nevin N. Naguib, Jeffrey W. Elam, James Birrell, Jian Wang, David S. Grierson, Bernd Kabius, Jon M. Hiller, Anirudha V. Sumant, Robert W. Carpick, Orlando Auciello, John A. Carlisle, "Enhanced nucleation, smoothness and conformality of ultrananocrystalline diamond (UNCD) ultrathin films via tungsten interlayers", *Chemical Physics Letters*, Vol. 430, Issues 4-6, p. 345-350, 2006.

[46] Satoshi Koizumi, Christoph Nebel, Milos Nesladek, Physics and Applications of CVD Diamond, John Wiley & Sons, 2008.

[47] L. Ostrovskaya, V. Perevertailo, V. Ralchenko, A. Dementjev, O. Loginova, "Wettability and surface energy of oxidized and hydrogen plasma-treated diamond films", *Diamond and Related Materials*, Vol. 11, p. 845-850, 2002.